Massively multiplexed nucleic acid detection using Cas13

nature

https://doi.org/10.1038/s41586-020-2279-8

Accelerated Article Preview

Massively multiplexed nucleic acid detection using Cas13

Received: 20 March 2019

Accepted: 20 April 2020

Accelerated Article Preview Published online 29 April 2020

Cite this article as: Ackerman, C. M. et al. Massively multiplexed nucleic acid detection using Cas13. *Nature* https://doi.org/10.1038/s41586-020-2279-8 (2020).

Open access

Cheri M. Ackerman, Cameron Myhrvold, Sri Gowtham Thakku, Catherine A. Freije, Hayden C. Metsky, David K. Yang, Simon H. Ye, Chloe K. Boehm, Tinna-Sólveig F. Kosoko-Thoroddsen, Jared Kehe, Tien G. Nguyen, Amber Carter, Anthony Kulesa, John R. Barnes, Vivien G. Dugan, Deborah T. Hung, Paul C. Blainey & Pardis C. Sabeti

Article

Massively multiplexed nucleic acid detection using Cas13

https://doi.org/10.1038/s41586-020-2279-8

Received: 20 March 2019

Accepted: 20 April 2020

Published online: 29 April 2020

Open access

Cheri M. Ackerman[1,2,12], Cameron Myhrvold[1,3,12]✉, Sri Gowtham Thakku[1,4], Catherine A. Freije[1,5], Hayden C. Metsky[1,6], David K. Yang[1], Simon H. Ye[1,4], Chloe K. Boehm[1], Tinna-Sólveig F. Kosoko-Thoroddsen[1], Jared Kehe[1,2], Tien G. Nguyen[1], Amber Carter[1], Anthony Kulesa[1,2], John R. Barnes[7], Vivien G. Dugan[7], Deborah T. Hung[1,8], Paul C. Blainey[1,2,9,13]✉ & Pardis C. Sabeti[1,3,10,11,13]

The overwhelming majority of globally circulating pathogens go undetected, undermining patient care and hindering outbreak preparedness and response. To enable routine surveillance and comprehensive diagnostic applications, there is a need for detection technologies that can scale to test many samples[1–3] while simultaneously testing for many pathogens[4–6]. Here, we develop Combinatorial Arrayed Reactions for Multiplexed Evaluation of Nucleic acids (CARMEN), a platform for scalable, multiplexed pathogen detection. In the CARMEN platform, nanoliter droplets containing CRISPR-based nucleic acid detection reagents[7] self-organize in a microwell array[8] to pair with droplets of amplified samples, testing each sample against each CRISPR RNA (crRNA) in replicate. The combination of CARMEN and Cas13 detection (CARMEN-Cas13) enables robust testing of >4,500 crRNA-target pairs on a single array. Using CARMEN-Cas13, we developed a multiplexed assay that simultaneously differentiates all 169 human-associated viruses with ≥10 published genome sequences and rapidly incorporated an additional crRNA to detect the causative agent of the 2020 COVID-19 pandemic. CARMEN-Cas13 further enables comprehensive subtyping of influenza A strains and multiplexed identification of dozens of HIV drug-resistance mutations. CARMEN's intrinsic multiplexing and throughput capabilities make it practical to scale, as miniaturization decreases reagent cost per test >300-fold. Scalable, highly-multiplexed CRISPR-based nucleic acid detection shifts diagnostic and surveillance efforts from targeted testing of high-priority samples to comprehensive testing of large sample sets, greatly benefiting patients and public health[9–11].

Infectious diseases are some of the greatest threats to human health and global security, yet there is no broadly available molecular test for the vast majority of disease-causing microbes, limiting their diagnosis and surveillance. Of the myriad viral species capable of infecting humans (576 of which had been sequenced, 169 of which had ≥10 published genomes in Oct 2018), only 39 had FDA-approved diagnostics[12,13]. While laboratory developed tests (LDTs) have been developed for clinical testing of diverse pathogens at specific facilities, these tests can have long turnaround times and are rarely multiplexed. Routine comprehensive diagnostic testing would provide a previously unavailable data stream to inform patients, healthcare workers, and policy makers to suppress and mitigate outbreaks. However, these tools are not widely available due to the lack of a scalable and multiplexed technology to quickly and inexpensively identify any circulating pathogen (Fig. 1A). Comprehensive disease detection by sequencing or microarray hybridization provides exquisite information about pathogen genotypes and evolution, but is difficult to implement on a broad scale due to the cost and logistical demands of sample preparation[4–6,14]. On the other hand, rapid, low-cost detection methods, such as CRISPR-based approaches, antigen-based tests, PCR, or LAMP, detect only one or a handful of pathogens in a given reaction[1–3,7,15–17]. Combining the strengths of these approaches, an ideal diagnostic and surveillance technology would be highly multiplexed and easily scale across hundreds of samples.

Miniaturized and self-organizing microfluidic technology enables massive multiplexing of biochemical and cellular assays[18–22]. Recently, we developed a microwell array system that harnesses miniaturization

[1]Broad Institute of Massachusetts Institute of Technology (MIT) and Harvard, Cambridge, MA, USA. [2]Department of Biological Engineering, MIT, Cambridge, MA, USA. [3]Department of Organismic and Evolutionary Biology, Harvard University, Cambridge, MA, USA. [4]Division of Health Sciences and Technology, Harvard Medical School and MIT, Cambridge, MA, USA. [5]PhD Program in Virology, Division of Medical Sciences, Harvard Medical School, Boston, MA, USA. [6]Department of Electrical Engineering and Computer Science, MIT, Cambridge, MA, USA. [7]Influenza Division, Centers for Disease Control and Prevention, Atlanta, GA, USA. [8]Molecular Biology Department and Center for Computational and Integrative Biology, Massachusetts General Hospital, Boston, MA, USA. [9]Koch Institute for Integrative Cancer Research at MIT, Cambridge, MA, USA. [10]Howard Hughes Medical Institute (HHMI), Chevy Chase, MD, USA. [11]Department of Immunology and Infectious Disease, Harvard T. H. Chan School of Public Health, Boston, MA, USA. [12]These authors contributed equally: Cheri M. Ackerman, Cameron Myhrvold. [13]These authors jointly supervised this work: Paul C. Blainey, Pardis C. Sabeti. ✉e-mail: cmyhrvol@broadinstitute.org; pblainey@broadinstitute.org

and self-organization to perform comprehensive combinatorial experiments. In this system, the user prepares a collection of inputs as droplet emulsions, and the input droplets organize themselves in the wells of the array, creating all possible pairwise combinations in replicate without additional user effort or active instrumentation[8]. We envisioned that CRISPR-based nucleic acid detection could be integrated with the microwell array system to test many amplified samples for many analytes in parallel.

To enable highly multiplexed nucleic acid detection, we developed Combinatorial Arrayed Reactions for Multiplexed Evaluation of Nucleic acids (CARMEN; Fig. 1b and Extended Data Fig. 1). The inputs to CARMEN-Cas13 are samples amplified by PCR or Recombinase Polymerase Amplification (RPA) and Cas13 detection mixes, which contain Cas13, a sequence-specific CRISPR RNA (crRNA), and a cleavage reporter (Extended Data Fig. 1)[7]. Each amplified sample or detection mix is prepared in a conventional microtiter plate and combined with a distinct, solution-based fluorescent color code that serves as an optical identifier. Each color-coded solution is emulsified in fluorous oil to yield 1 nl droplets. Once emulsified, droplets from all samples and detection mixes are pooled into a single tube and, in one pipetting step, are loaded into a microwell array chip molded from polydimethylsiloxane (PDMS) (Fig. 1b and Extended Data Fig. 1-2). Each microwell in the array accommodates two droplets from the pool at random, thereby spontaneously forming all pairwise combinations of dropletized inputs, and the array is sealed against a glass substrate to physically isolate each microwell. The contents of each microwell are determined by identifying the color codes of the droplets using fluorescence microscopy. Exposure to an electric field merges the droplet pairs confined in each microwell and initiates all detection reactions simultaneously. Fluorescence microscopy is used to monitor each detection reaction (Fig. 1b and Extended Data Fig. 1-2).

CARMEN-Cas13 is sensitive, specific, and statistically robust. CARMEN-Cas13 detects Zika sequences with attomolar sensitivity, harnessing the collateral cleavage activity[23,24] of CRISPR-Cas13 to match the sensitivity of Specific High-sensitivity Enzymatic Reporter unLOCKing (SHERLOCK) and PCR-based assays (Fig. 1c, Extended Data Fig. 3, and Supplementary Discussion I)[7,17]. Additionally, CARMEN-Cas13 benefits from the specificity of SHERLOCK: sequence-specific identification is achieved through Cas13-crRNA binding and recognition, alleviating concerns about off-target amplification that are common in other nucleic acid detection methods (Supplementary Discussion II). Each CARMEN-Cas13 assay combines M samples and N crRNAs to perform MxN 'tests'; each test comprising a set of crRNA-sample droplet pair replicates (Supplementary Discussion III). The droplet-level CARMEN-Cas13 reactions are highly reproducible themselves, enabling 1,000 tests per standard-capacity chip (Extended Data Fig. 3 and Supplementary Discussion IV).

Accurate testing of multiple samples for hundreds of microbial pathogens demands higher throughput than existing multiplexed detection systems offer[2,25,26]. To enable highly-multiplexed detection with high sample throughput, we developed a set of 1,050 solution-based color codes using ratios of 4 commercially-available, small-molecule fluorophores. Using the 1,050 color codes, 99.5% of droplets can be correctly classified after permissive filtering that retains 94% of droplets (Extended Data Fig. 4 and Supplementary Discussion V). To match the throughput enabled by our 1,050 color codes, we designed a massive-capacity chip (mChip) that allows >4,500 statistically replicated tests per chip (Extended Data Fig. 5). mChip reduces the reagent cost per test >300-fold relative to standard well-plate SHERLOCK tests, while reducing pipetting steps and turnaround time (Extended Data Table 1 and Supplementary Discussion VI-VII).

We designed a CARMEN-Cas13 assay to selectively and simultaneously test dozens of samples for all 169 human-associated viruses (HVs) with ≥10 available, published genomes (as of October 24, 2018). We applied ADAPT (Metsky et al. *in prep*) to the published viral genomes of viruses represented in our HV panel to select amplicons for PCR primer pools, using primer3 to optimize primer sequences[27]. ADAPT accepts a collection of sequences arranged into groups (e.g., all known sequences within a species). For each group, ADAPT searches for an optimal set of crRNAs that are sensitive to the sequences within the group (i.e., detect a desired fraction of sequences) and are unlikely to detect sequences in the other groups (Extended Data Fig. 5h). We used ADAPT to design a small set of crRNA sequences for each species such that, accounting for genome diversity on NCBI GenBank, each crRNA set provides high coverage (>90% of sequences detected) within its targeted species and high selectivity against other species (Fig. 2a, Extended Data Fig. 5). We designed the HV panel as a modular master set of nucleic acid detection assays which can be customized by the end user for diverse applications (Fig. 2a).

Taking advantage of CARMEN-Cas13's massive multiplexing capabilities, we tested the full HV panel and demonstrated its performance. We computationally selected the optimal crRNA from each species set in the design (169 total, see Supplementary Discussion IX.A) and evaluated each against synthetic consensus sequences for every species, which had each been amplified using its corresponding primer pool (184 total PCR products, including controls; Fig. 2b), for a total of 30,912 tests performed across 8 mChips (see Supplementary Table 1). We performed two rounds of testing, improving the designs for 11 species (6.5%) for the second round. We observed 97.2% concordance between the two rounds for unchanged designs, demonstrating that individual crRNAs can be improved without altering the performance of the rest of the assay (Extended Data Fig. 6, Supplementary Discussion IX, and Supplementary Data File 3). In round two, 157 of 167 (94%) of crRNAs were selective for their targets with signal above threshold (6 standard deviations above background), with a median AUC of 0.997 across all 167 crRNAs (Extended Data Fig. 6). Furthermore, widespread cross-reactivity is not observed, even when synthetic targets are amplified with all primer pools (Extended Data Fig. 7).

As an outbreak of COVID-19 emerged during the manuscript review process, we rapidly incorporated a new test[28] for the novel coronavirus (nCoV) SARS-CoV-2 into a coronavirus panel taken from the HV panel, demonstrating the power of this modular master set to be adapted to real-world challenges (Fig. 2d). Using a single mChip, >400 samples can be tested in parallel against our coronavirus panel.

To test CARMEN in a more challenging context, we evaluated the HV panel against 58 plasma, serum, and throat/nasal swab samples from patients with a variety of confirmed infections. Each clinical sample was treated as an unknown and amplified using all 15 primer pools (Fig. 2e, Extended Data Fig. 7a). To increase testing throughput, PCR products were subsequently pooled in sets of 3 (5 "metapools" per patient sample) and tested with crRNAs from the HV panel (Extended Data Fig. 8a). As a gold-standard comparative readout, next generation sequencing (NGS) was performed with >2 million reads per sample; of the 11,268 tests that were interpretable by both methods, 11,236 (99.7%) were concordant (Fig. 2f). We found that CARMEN identified the known infection in the majority of samples where NGS detected any sequences from these viruses, including complete concordance between CARMEN and NGS for dengue and Zika tests (Fig. 2g). CARMEN and NGS can also be compared based on their ability to detect the sequence locus targeted by the CARMEN crRNA, revealing that CARMEN is more sensitive than NGS on a per-sequence locus basis among the crRNA targets tested (Fig. 2h and Extended Data Fig. 8b). CARMEN's overall sensitivity of detection, especially for diverse viruses, can be increased by the addition of crRNAs to cover additional loci and/or loci with sequence diversity, as we demonstrate with influenza A subtyping in Fig. 3. Notably, sequence heterogeneity at the target locus is a challenge that all targeted nucleic acid detection methods face, and CARMEN can overcome this through crRNA multiplexing.

Finally, during our patient sample testing, both CARMEN and NGS identified specific viruses not previously known to exist in the samples (Fig. 2i and Extended Data Figure 8b). Thus, while it is clear the HV panel can be applied for surveillance of many viruses in parallel, it is important to recognize that integrating results from the HV panel with patient symptoms and medical expertise will be critical for the effective use of CARMEN testing in clinical settings.

Capitalizing on the specificity of Cas13 detection, we used CARMEN-Cas13 to discriminate all epidemiologically relevant serotypes of influenza A in parallel. Diversity within a viral species, such as influenza A, poses a significant challenge to detection: an assay must correctly identify many distinct sequences within a group of strains, while remaining selective for that group. To discriminate the hemagglutinin (H) and neuraminidase (N) subtypes H1-H16 and N1-N9 of influenza A virus, we designed H and N amplicons that were sufficiently conserved to amplify with two parallel primer sets and used ADAPT to design specific sets of crRNAs to identify subtypes (Fig. 3a, see Methods for details). We tested the optimal crRNA from each set using synthetic consensus sequences from H1-16 and N1-9, and readily identified these subtypes (Fig. 3b-c). We further tested our N subtyping assay using synthetic sequences which collectively cover >90% of the sequence diversity within subtypes N1-9, and identified 32 out of 35 (91.4%) of these sequences (Extended Data Fig. 8c). Finally, we validated our subtyping assay using 20 throat and nasal swabs from humans infected during the 2018-19 flu season and were able to successfully subtype all of these infections, showing 100% concordance with RT-qPCR performed by the CDC and NGS performed in our laboratory (Fig. 3d, Supplementary Methods III.C). Based on these results, our assay could potentially identify each of the 144 possible combinations of H1-16 and N1-9 subtypes.

The exquisite specificity of Cas13 also enables CARMEN-Cas13 to identify clinically relevant viral mutations in multiplex, such as those that confer drug resistance. To demonstrate this, we designed primer pairs tiling the HIV reverse transcriptase (RT) coding sequence and a set of crRNAs to identify six drug resistance mutations (DRMs, Fig. 4a, Supplementary Table 2) that are prevalent in antiviral-naive patient populations[29]. Testing our designs against synthetic targets, we identified all 6 mutations in parallel (Fig. 4b, Extended Data Fig. 9a). We validated our RT DRM assay on 22 samples from patients with HIV, some of which contained multiple mutations (Extended Data Fig. 9b), and demonstrated 90% concordance with Sanger sequencing results from the sample provider and 86% concordance with NGS we performed in parallel with CARMEN testing. In some cases, NGS revealed differences between our primer and crRNA designs and patient sequences, as we designed our assay against HIV subtype B, but tested it using samples obtained later from patients infected with HIV subtype G. Filtering by sequences with ≤3 mismatches relative to our design increased the concordance between CARMEN and Sanger sequencing (93%) and the concordance between CARMEN and NGS (93%) (Fig. 4c-d). To demonstrate the generalizability of our approach, we developed a CARMEN panel to test for 21 clinically-relevant DRMs in HIV integrase[30], the target of front-line HIV therapy, and identified all of these mutations in a set of 9 composite synthetic targets (Fig. 4e, Supplementary Table 2).

We have demonstrated a broad set of uses for CARMEN-Cas13—differentiating viral sequences at the species, strain, and SNP levels—and the capability to rapidly develop and validate highly multiplexed detection panels. More generally, CARMEN-Cas13 augments CRISPR-based nucleic acid detection technologies by increasing throughput, decreasing reagent and sample consumption per test, and enabling detection over a larger dynamic range (Extended Data Fig. 9c-d). The flexibility and high throughput of CARMEN can accommodate the addition and rapid optimization of new amplification primers or crRNAs to existing CARMEN assays to facilitate detection of newly discovered pathogen sequences, as we demonstrated for SARS-CoV-2. Additionally, in the broader context of pathogen detection, discovery, and evolution, CARMEN and next-generation sequencing complement each other. CARMEN can rapidly identify infected samples for further sequencing to track the ongoing evolution of the virus, and newly identified sequences can inform the design of improved CRISPR-based diagnostics. In the future, we imagine region- and outbreak-specific detection panels deployed to test thousands of samples from selected populations, including animal vectors, animal reservoirs, or patients presenting with symptoms. The adoption of such panels in connection with clinical care will require careful contextualized interpretation of results by experts. CARMEN unleashes CRISPR-based diagnostics at scale, a critical step toward routine, comprehensive disease surveillance to improve patient care and public health.

Online content

Any methods, additional references, Nature Research reporting summaries, source data, extended data, supplementary information, acknowledgements, peer review information; details of author contributions and competing interests; and statements of data and code availability are available at https://doi.org/10.1038/s41586-020-2279-8.

1. Bosch, I. *et al*. Rapid antigen tests for dengue virus serotypes and Zika virus in patient serum. *Sci. Transl. Med*. **9**, (2017).
2. Popowitch, E. B., O'Neill, S. S. & Miller, M. B. Comparison of the Biofire FilmArray RP, Genmark eSensor RVP, Luminex xTAG RVPv1, and Luminex xTAG RVP fast multiplex assays for detection of respiratory viruses. *J. Clin. Microbiol*. **51**, 1528–1533 (2013).
3. Du, Y. *et al*. Coupling Sensitive Nucleic Acid Amplification with Commercial Pregnancy Test Strips. *Angew. Chem. Int. Ed Engl*. **56**, 992–996 (2017).
4. Wang, D. *et al*. Microarray-based detection and genotyping of viral pathogens. *Proc. Natl. Acad. Sci. U. S. A*. **99**, 15687–15692 (2002).
5. Houldcroft, C. J., Beale, M. A. & Breuer, J. Clinical and biological insights from viral genome sequencing. *Nat. Rev. Microbiol*. **15**, 183–192 (2017).
6. Palacios, G. *et al*. Panmicrobial oligonucleotide array for diagnosis of infectious diseases. *Emerg. Infect. Dis*. **13**, 73–81 (2007).
7. Gootenberg, J. S. *et al*. Nucleic acid detection with CRISPR-Cas13a/C2c2. *Science* **356**, 438–442 (2017).
8. Kulesa, A., Kehe, J., Hurtado, J. E., Tawde, P. & Blainey, P. C. Combinatorial drug discovery in nanoliter droplets. *Proc. Natl. Acad. Sci. U. S. A*. **115**, 6685–6690 (2018).
9. Chertow, D. S. Next-generation diagnostics with CRISPR. *Science* **360**, 381–382 (2018).
10. Kocak, D. D. & Gersbach, C. A. From CRISPR scissors to virus sensors. *Nature* **vol. 557** 168–169 (2018).
11. Bordi, L. *et al*. Differential diagnosis of illness in patients under investigation for the novel coronavirus (SARS-CoV-2), Italy, February 2020. *Eurosurveillance* **25**, 2000170 (2020).
12. US Food & Drug Administration. www.fda.gov.
13. Brister, J. R., Rodney Brister, J., Ako-adjei, D., Bao, Y. & Blinkova, O. NCBI Viral Genomes Resource. *Nucleic Acids Res*. **43**, D571–D577 (2014).
14. Briese, T. *et al*. Virome Capture Sequencing Enables Sensitive Viral Diagnosis and Comprehensive Virome Analysis. *MBio* **6**, e01491–15 (2015).
15. Chen, J. S. *et al*. CRISPR-Cas12a target binding unleashes indiscriminate single-stranded DNase activity. *Science* **360**, 436–439 (2018).
16. Gootenberg, J. S. *et al*. Multiplexed and portable nucleic acid detection platform with Cas13, Cas12a, and Csm6. *Science* **360**, 439–444 (2018).
17. Myhrvold, C. *et al*. Field-deployable viral diagnostics using CRISPR-Cas13. *Science* **360**, 444–448 (2018).
18. Macosko, E. Z. *et al*. Highly Parallel Genome-wide Expression Profiling of Individual Cells Using Nanoliter Droplets. *Cell* **161**, 1202–1214 (2015).
19. Quake, S. Solving the Tyranny of Pipetting. *arXiv* (2018).
20. Ismagilov, R. F., Ng, J. M., Kenis, P. J. & Whitesides, G. M. Microfluidic arrays of fluid-fluid diffusional contacts as detection elements and combinatorial tools. *Anal. Chem*. **73**, 5207–5213 (2001).
21. Thorsen, T., Maerkl, S. J., Quake, S. R. Microfluidic Large-Scale Integration. *Science* **298**, 580–584 (2002).
22. Jackman, R. J., Duffy, D. C., Ostuni, E., Willmore, N. D. & Whitesides, G. M. Fabricating large arrays of microwells with arbitrary dimensions and filling them using discontinuous dewetting. *Anal. Chem*. **70**, 2280–2287 (1998).
23. Abudayyeh, O. O. *et al*. C2c2 is a single-component programmable RNA-guided RNA-targeting CRISPR effector. *Science* **353**, aaf5573 (2016).
24. East-Seletsky, A. *et al*. Two distinct RNase activities of CRISPR-C2c2 enable guide-RNA processing and RNA detection. *Nature* **538**, 270–273 (2016).
25. Hassibi, A. *et al*. Multiplexed identification, quantification and genotyping of infectious agents using a semiconductor biochip. *Nat. Biotechnol*. **36**, 738–745 (2018).
26. Dunbar, S. A. Applications of Luminex xMAP technology for rapid, high-throughput multiplexed nucleic acid detection. *Clin. Chim. Acta* **363**, 71–82 (2006).
27. Untergasser, A. *et al*. Primer3—new capabilities and interfaces. *Nucleic Acids Res*. **40**, e115–e115 (2012).

28. Metsky, H. C., Freije, C. A., Kosoko-Thoroddsen, T.-S. F., Sabeti, P. C. & Myhrvold, C. CRISPR-based surveillance for COVID-19 using genomically-comprehensive machine learning design. *bioRxiv* 2020.02.26.967026 (2020) https://doi.org/10.1101/2020.02.26.967026.
29. Gupta, R. K. *et al*. HIV-1 drug resistance before initiation or re-initiation of first-line antiretroviral therapy in low-income and middle-income countries: a systematic review and meta-regression analysis. *Lancet Infect. Dis*. **18**, 346–355 (2018).
30. Wensing, A. M. *et al*. 2017 Update of the Drug Resistance Mutations in HIV-1. *Top. Antivir. Med*. **24**, 132–133 (2017).

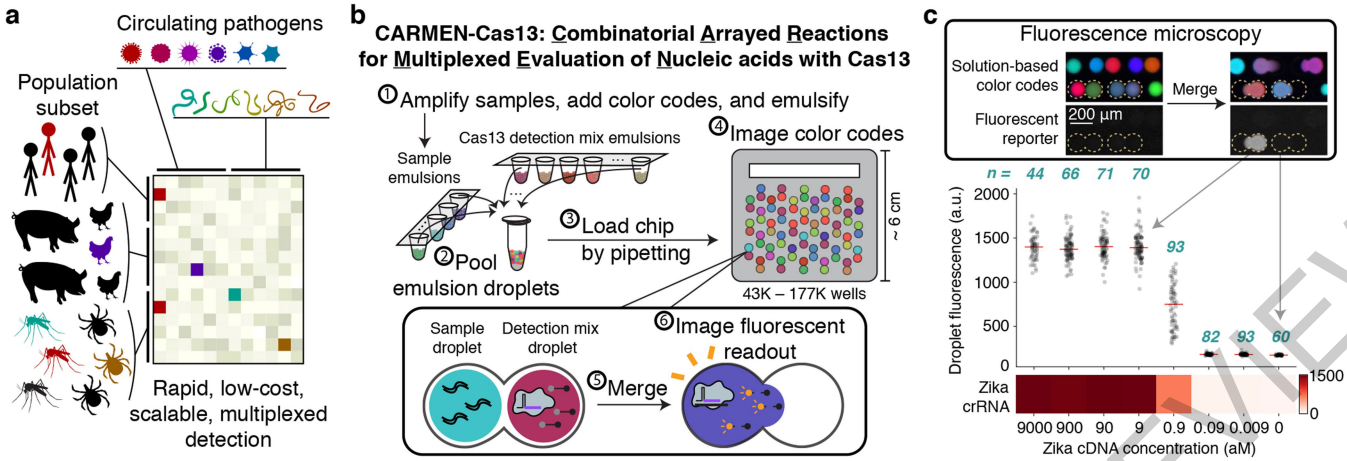

Fig. 1 | Combinatorial Arrayed Reactions for Multiplexed Evaluation of Nucleic acids with Cas13 (CARMEN-Cas13) achieves attomolar sensitivity. **a**, Identification of multiple circulating pathogens in human and animal populations represents a large-scale detection problem. **b**, Schematic of CARMEN-Cas13 workflow. **c**, Zika cDNA is detected by a single CARMEN-Cas13 assay with attomolar sensitivity and tens of replicate droplet pairs (black dots, numbers of replicates are in blue); red lines mark medians in the graph and are used to construct the heatmap below. Representative droplet images are shown above the graph.

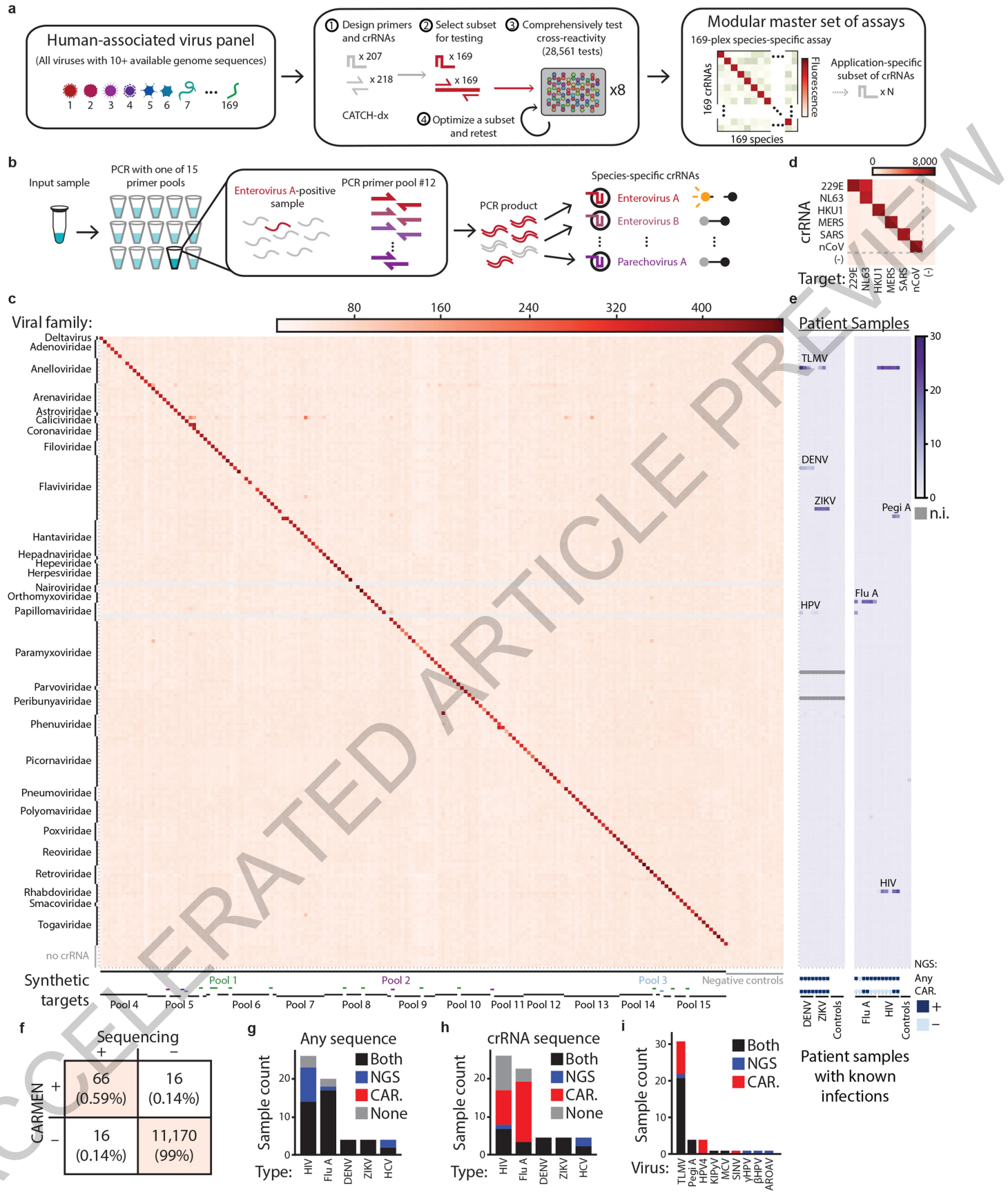

Fig. 2 | See next page for caption.

Fig. 2 | Comprehensive identification of human-associated viruses with CARMEN-Cas13. a, The development and testing of a panel for all 169 human-associated viruses with ≥10 available genome sequences. **b**, Experimental design using pooled PCR amplification. **c**, Testing a comprehensive human-associated viral (HV) panel with synthetic targets using CARMEN-Cas13. PCR primer pools and viral families are below and to the left of the heatmap, respectively. Gray lines: crRNAs not tested. **d**, Multiplexed coronavirus panel. 229E, NL63, HKU1: human coronaviruses 229E, NL63, and HKU1; MERS: Middle East respiratory syndrome coronavirus; SARS: severe acute respiratory syndrome coronavirus; nCoV: novel coronavirus SARS-CoV-2. **e**, Testing the HV panel with patient samples (additional data: Extended Data Fig. 8a). Heatmaps indicate background-subtracted fluorescence after 1 h (**c**) or 30 min (**d**), or fold-change over background (**e**). **f**, Concordance of CARMEN and NGS for patient sample testing. Each box displays the number of tests and the percent of the total. **g**, Identification by NGS or CARMEN of any viral sequence from the known infections in patient samples (e.g. HIV test results for HIV samples). **h**, Identification by NGS or CARMEN of the crRNA target for each known infection. **i**, Positive test results in patient samples for viruses other than the known infections. In **g**-**i**, Black: detected by CARMEN and NGS; Blue: detected by NGS only; Red: detected by CARMEN only; Gray: not detected by CARMEN or NGS. DENV: dengue virus; ZIKV: Zika virus; HCV: hepatitis C virus; TLMV: Torque teno-like mini virus; Pegi A: pegivirus A; HPV4: human papillomavirus 4; KIPyV: KI polyomavirus; MCV: Merkel cell polyomavirus; SINV: Sindbis virus, γHPV: gamma human papillomavirus; βHPV: beta human papillomavirus 2; AROAV: aroa virus (Note: CARMEN does not test for γHPV or AROAV because fewer than 10 γHPV or AROAV genomes had been published before Oct 24, 2018).

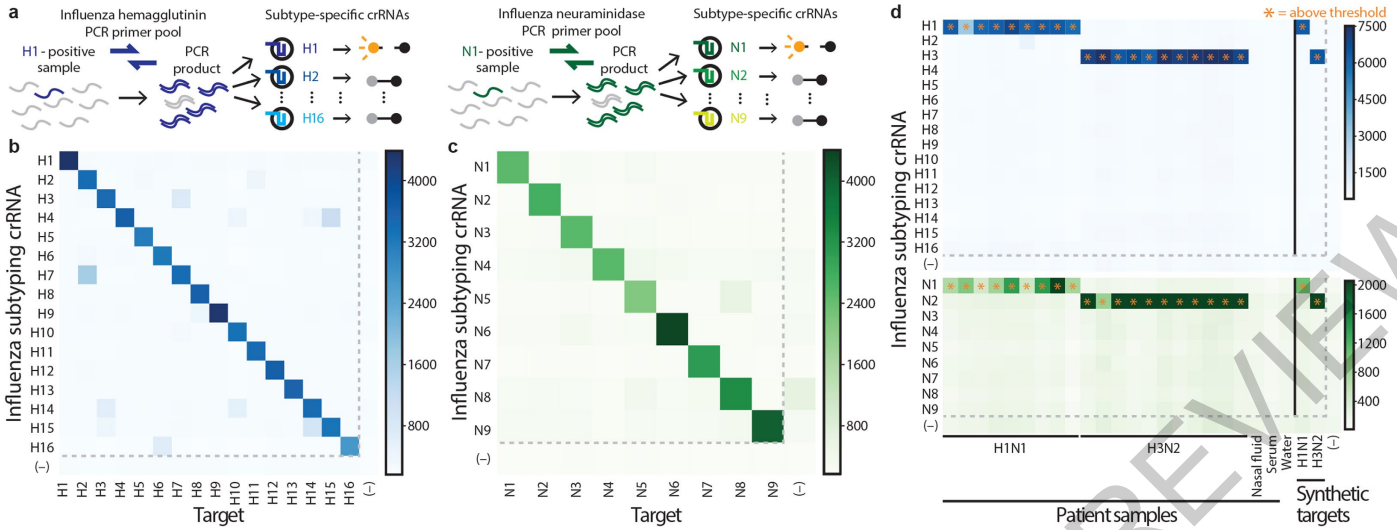

Fig. 3 | Influenza subtype discrimination with CARMEN-Cas13. a, Schematic of influenza A subtype discrimination using CARMEN-Cas13. **b**, Discrimination of H1-H16 using CARMEN-Cas13. **c**, Discrimination of N1-N9 using CARMEN-Cas13. **d**, Identification of H and N subtypes from patient samples and mixed synthetic targets (Supplementary Methods III.C). Heatmaps indicate background-subtracted fluorescence after 1 h (for H1-16 discrimination) or 3 h (for N1-9 discrimination) of Cas13 detection. In (**b**-**d**), synthetic targets were used at 10^4 cp/µl. Asterisks in (**d**) indicate a signal above threshold for a synthetic target or patient sample.

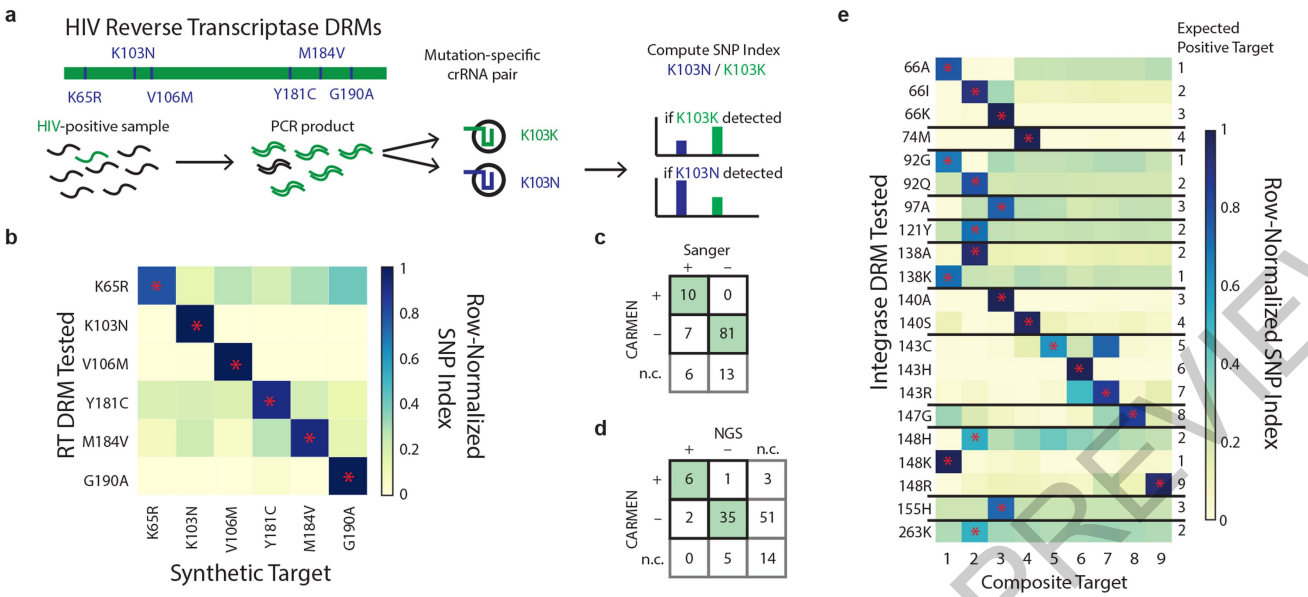

Fig. 4 | Multiplexed DRM identification with CARMEN-Cas13. a, Schematic of HIV drug resistance mutation (DRM) identification using CARMEN-Cas13. **b**, Identification of 6 reverse transcriptase mutations using CARMEN-Cas13. Concordance between **c**, CARMEN-Cas13 and Sanger-sequencing, or **d**, CARMEN-Cas13 and NGS, for DRM identification in patient plasma or serum samples for sequences with ≤3 mismatches relative to our design. **e**, Identification of 21 integrase DRMs using CARMEN-Cas13. Heatmaps indicate SNP indexes after 0.5-3 h of Cas13 detection, normalized by row. In (**b** and **e**), synthetic targets were used at 10^4 cp/µl. Asterisks indicate the synthetic target with the mutation.

Methods

I. Ethics Statement

Human samples from dengue, HCV, HIV, and Zika patients were obtained commercially from Boca Biolistics under their ethical approvals. Influenza samples were obtained from the Centers for Disease Control and Prevention (CDC) under their ethical approvals. All protocols subsequently performed by the researchers were approved as a Not Human Subjects Research determination #NHSR-4318 issued by the Broad Institute of MIT and Harvard.

II. General experimental procedure

II.A. Preparation of synthetic targets, patient samples, and crRNAs

Synthetic targets. Synthetic DNA targets were ordered from Integrated DNA Technologies (IDT) and resuspended in nuclease-free water. Resuspended DNA was serially diluted to 10^4 copies per microliter and used as inputs to PCR or RPA reactions.

CARMEN sample preparation. For all clinical samples and healthy human plasma, serum, urine, and nasal fluid, RNA was extracted from 140 µl of input material using the QIAamp Viral RNA Mini Kit (QIAGEN) with carrier RNA according to the manufacturer's instructions. Samples were eluted in 60 µl of nuclease free water and stored at -80 °C until use. 10 µl of extracted RNA was converted into single-stranded cDNA in a 40 µl reaction. First, random hexamer primers were annealed to sample RNA at 70 °C for 7 minutes followed by reverse transcription using SuperScript IV (Invitrogen) with random hexamer primers for 20 minutes at 55 °C. cDNA was stored at -20 °C until use. DNase treatment was not performed at any point during sample preparation.

Sequencing library preparation. Extracted viral nucleic acids were prepared for sequencing using library construction methods that have been previously described with a few differences noted below[31]. Following extraction, double-stranded complementary DNA (cDNA) was created using random primers and SuperScript IV (Thermo Fisher Scientific) for first-strand synthesis and *E. coli* polymerase I (NEB) for second-strand synthesis. Sequencing libraries were generated using the Nextera XT DNA Library Prep Kit (Illumina) with 10-16 cycles of PCR to introduce unique dual index pairs. Libraries were then quantified using the KAPA Universal Complete Kit (Roche) and 12-18 samples were pooled for sequencing including a no input negative control. Samples were sequenced to >0.82 M read-mates using 2×75 bp paired-end reads from the Illumina NextSeq Reagent Kit v2.5.

crRNA preparation. For viral detection (Figs 1–3), crRNAs were synthesized by Synthego and resuspended in nuclease-free water. For SNP detection (Fig. 4), crRNA DNA templates were annealed to a T7 promoter oligonucleotide at a final concentration of 10 µM in 1× Taq reaction buffer (New England Biolabs). This procedure involved 5 minutes of initial denaturation at 95 °C, followed by an anneal at 5 °C per minute down to 4 °C. SNP detection crRNAs were transcribed from annealed DNA templates *in vitro* using the HiScribe T7 High Yield RNA Synthesis Kit (New England Biolabs). Transcriptions were performed according to the manufacturer's instructions for short RNA transcripts, with the volume scaled to 30 µl. Reactions were incubated for 18 hours or overnight at 37 °C. Transcripts were purified using RNAClean XP beads (Beckman Coulter) with a 2× ratio of beads to reaction volume and an additional supplementation of 1.8× isopropanol and resuspended in nuclease-free water. *In vitro* transcribed RNA products were then quantified using a NanoDrop One (Thermo Scientific) or on a Take3 plate with absorbance measured by a Cytation 5 (Biotek Instruments). Cas13a was recombinantly expressed and purified as described by Genscript, and was stored in Storage Buffer (600 mM NaCl, 50 mM Tris-HCl pH 7.5, 5% glycerol, 2mM DTT)[7].

II.B. Nucleic acid amplification.

Unless specified otherwise, amplification was performed by PCR using Q5 Hot Start polymerase (New England Biolabs) using primer pools (with 150 nM of each primer) in 20 µl reactions. Amplified samples were stored at -20 °C until use. For details about thermal cycling conditions, see Sections III.B-III.D.

II.C. Cas13 detection reactions

Cas13 detection reactions. Detection assays were performed with 45 nM purified *Lwa*Cas13a, 22.5 nM crRNA, 500 nM quenched fluorescent RNA reporter (RNAse Alert v2, Thermo Scientific), 2 µl murine RNase inhibitor (New England Biolabs) in nuclease assay buffer (40 mM Tris-HCl, 60 mM NaCl, pH 7.3) with 1 mM ATP, 1 mM GTP, 1 mM UTP, 1 mM CTP, and 0.6 µl T7 polymerase mix (Lucigen). Input of amplified nucleic acid varied by assay with details described in Section III. Detection mixes were prepared as 2.2× master mix, such that each droplet contained a 2× master mix after color coding and a 1× master mix after droplet merging.

II.D. Color coding, emulsification, and droplet pooling

Color coding. Unless specified otherwise, amplified samples were diluted 1:10 into nuclease-free water supplemented with 13.2 mM $MgCl_2$ prior to color coding to achieve a final concentration of 6 mM after droplet merging. Detection mixes were not diluted. Color code stocks (2 µl) were arrayed in 96W plates (for detailed information on construction of color codes, see Section V.B., below). Each amplified sample or detection mix (18 µl) was added to a distinct color code and mixed by pipetting.

Emulsification. The color-coded reagents (20 µl) and 2% 008-fluorosurfactant (RAN Biotechnologies) in fluorous oil (3M 7500, 70 µl) were added to a droplet generator cartridge (Bio Rad), and reagents were emulsified into droplets using a Bio Rad QX200 droplet generator or a custom aluminum pressure manifold.

Droplet pooling. A total droplet pool volume of 150 µl of droplets was used to load each standard chip; a total of 800 µl of droplets was used to load each mChip. To maximize the probability of forming productive droplet pairings (amplified sample droplet + detection reagent droplet), half the total droplet pool volume was devoted to target droplets and half to detection reagent droplets. For pooling, individual droplet mixes were arrayed in 96W plates. A multichannel pipet was used to transfer the requisite volumes of each droplet type into a single row of 8 droplet pools, which were further combined to make a single droplet pool. The final droplet pool was pipetted up and down gently to fully randomize the arrangement of the droplets in the pool. The pooling step is rapid (<10 min), and small molecule exchange between droplets during this period does not significantly alter the color codes (see Supplementary Discussion).

II.E. Loading, imaging, and merging microwell arrays

Microwell array loading (standard chips). Loading of standard chips was performed as described previously[36]. Briefly, each chip was placed into an acrylic chip-loader, such that the chip was suspended ~300-500 µm above the surface of hydrophobic glass, creating a flow space between the chip and the glass. The flow space was filled with fluorous oil (3M, 7500) until loading; immediately before loading, fluorous oil was drained from the flow space. In a single pipetting step, the droplet pool was added to the flow space (Extended Data Fig. 2, step 3). The loader was tilted to move the droplet pool within the flow space until the microwells were filled with droplets. Fresh fluorous oil (3M 7500) without surfactant was used to wash the flow space (3 × 1 ml), the flow space was filled with oil, and the chip was sealed against the glass by screwing the loader shut (Extended Data Fig. 2, step 4). Additional oil (1 ml) was added to the loading slot, and the slot was sealed with clear tape (Scotch) to prevent evaporation.

Microwell array loading (mChips). The back of an mChip was pressed against the lid of the mChip loader to adhere the chip to the lid and leave the microwell array facing out (Extended Data Fig. 5d, middle illustration). The lid was placed on the loader base, such that opposing

magnets in the lid and base held the lid and chip suspended above the base (Extended Data Fig. 5d, right illustration, and Extended Data Fig. 5f). Wingnuts on screws were used to push the lid toward the base until the flow space between the surface of the chip and base was ~300-500 µm (Extended Data Fig. 5d, right illustration). The flow space was filled with fluorous oil (3M, 7500) until loading; immediately before loading, fluorous oil was drained from the flow space. In a single pipetting step, the droplet pool was added to the flow space by pipetting along the edge of the chip (Extended Data Fig. 5f, step 3). The loader was tilted to move the droplet pool within the flow space until the microwells were filled with droplets. Fresh fluorous oil (3M 7500) without surfactant was used to wash the flow space (3 × 1 ml). Two pieces of PCR film (MicroAmp, Applied Biosystems) were joined by placing the sticky side of one piece a few millimeters over the edge of the other piece. The sheet of PCR film was wetted with fluorous oil and set aside. Returning to the loader: the wingnuts were removed so the lid of the loader (with the mChip attached) could be removed from the base. The mChip was sealed against the sheet of wet PCR film in a single smooth motion (Extended Data Fig. 5f, step 4). The excess PCR film hanging over the edges of the chip was trimmed with a razor blade.

Microwell array imaging, merging, and subsequent imaging. After chip loading, the color code of each droplet was identified by fluorescence microscopy (Extended Data Fig. 2, step 4, and Extended Data Fig. 5g). After imaging, the droplet pairs in each microwell were merged by passing the tip of a corona treater (Model BD-20, Electro-Technic Products) over the glass or PCR film (Extended Data Fig. 2, step 5). The merged droplets were immediately imaged by fluorescence microscopy (Extended Data Fig. 2, step 6) and placed in an incubator (37 ˚C) until subsequent imaging time points. All imaging was conducted on a Nikon TI2 microscope equipped with an automated stage (Ludl Electronics, Bio Precision 3 LM), LED light source (Lumencor, Sola), and camera (Hamamatsu, Orca Flash4.0, C11440, sCMOS). Unless otherwise noted, standard chips were imaged using a 2× objective (Nikon, MRD00025), while a 1× objective (Nikon, MRL00012) was used for mChips in order to reduce imaging time. The following filter cubes were used for imaging: Alexa Fluor 405: Semrock LED-DAPI-A-000; Alexa Fluor 555: Semrock SpGold-B; Alexa Fluor 594: Semrock 3FF03-575/25-25 + FF01-615/24-25; and Alexa Fluor 647: Semrock LF635-B. During imaging, the microscope condenser was tilted back to reduce background fluorescence in the 488 channel. Additionally, during experiments involving UV channel imaging, black cloth was draped over the microscope to reduce background fluorescence from light scattered off the ceiling.

II.F. Data analysis

Data analysis. Imaging data were analyzed with custom Python scripts. Analysis consisted of three parts: (1) pre-merge image analysis to determine the identity of the contents of each droplet based on droplet color codes; (2) post-merge image analysis to determine the fluorescence output of each droplet pair and map those fluorescence values back to the contents of the microwell; (3) statistical analysis of the data obtained in parts 1 and 2.

Pre-merge image analysis. The contents of each droplet were determined from images taken before droplet merging: a background image was subtracted from each droplet image, and fluorescence channel intensities were scaled so the intensity range of each channel was approximately the same. Droplets were identified using a Hough transform, and the fluorescence intensity of each channel at each droplet position was determined from a locally convolved image. Compensation for cross-channel optical bleed was applied, and all fluorescence intensities were normalized to the sum of the compensated 647 nm, 594 nm, and 555 nm channels. For 4-channel data sets, analysis of 3-color space was performed directly on normalized intensities. For 5-channel data sets, droplets were divided into UV intensity bins for downstream analysis (Extended Data Fig. 4). The 3-color space within each UV bin was analyzed separately. The 3-color intensity vectors for each droplet were projected onto the unit 2-simplex, and density-based spatial clustering of applications with noise (DBSCAN) was used to assign labels to each color code cluster. Manual clustering adjustments were made when necessary. For 5-channel data sets, UV intensity bins were recombined after assignments to create the full data set.

Post-merge image analysis. Background subtraction, intensity scaling, compensation, and normalization were performed as in pre-merge analysis. Following image registration of pre- and post-merge images, the fluorescence intensity of the reporter channel at each droplet pair position was determined from a locally convolved image. The physical mapping of the fluorescent reporter channel onto the previously determined positions of each color code served to assign the fluorescence signal in the reporter channel to the contents of each well. Quality filtering for appropriate post-merge droplet size (which excludes unmerged droplet pairs) and closeness of a droplet's color code to its designated color code cluster (see Extended Data Fig. 4) was applied.

Statistical analysis. Heat maps were generated from the median fluorescence value of each crRNA-Target pair. Performance of each guide was assessed by calculating a receiver operating characteristic (ROC) curve for the fluorescence distributions from on-target and all off-target droplets and determining the area under the curve (AUC).

SNP index calculation. The SNP index was calculated for each sample and each mutation by taking the ratio of the derived-allele-targeting crRNA and the ancestral-allele-targeting crRNA. In the heatmaps, SNP indexes were normalized by row (in Fig. 4b and 4d).

Sequencing data analysis. Reads aligning specifically to the human genome were filtered using KrakenUniq 0.5.8, then deduplicated using clumpify.sh 38.61. Remaining reads were aligned to a KrakenUniq database (link to database: gs://sabeti-public-dbs/krakenuniq/krakenuniq.full.20190626.tar.zst; link to library: gs://sabeti-public-dbs/krakenuniq/krakenuniq.full.library.20190626.tar.zst). The output of this was used to compute the number of reads per million (rpm), and ≥1 rpm was considered a positive result.

For viral genome assembly, reads were demultiplexed and analyzed using viral-ngs, which can be accessed at https://github.com/broadinstitute/viral-ngs/releases/tag/v1.25.0 (https://zenodo.org/record/3509008).

HIV genome assembly was scaffolded against GenBank accession AF063224.1, which was also used as the reference for aligning all HIV reads for those samples with or without full genome assemblies. Thirteen HIV samples had the sufficiently high read depth (≥2 unique reads) to make consensus base calls at one or more of the regions targeted by the SNP assays. Consensus base calls in these regions were used to confirm the presence or absence of the SNP and determine the number of mismatches between each sample's consensus HIV sequence and the crRNA. Each crRNA was aligned to each sample's consensus sequence, and the number of mismatches was calculated excluding the synthetic mismatch, SNP-induced mismatch, or any mismatches that were G-U wobble base pairs from the total number. The 'align_and_plot_coverage' function in viral-ngs (wrapping BWA-MEM[32], with options '--excludeDuplicates --minScoreToFilter 60') was used to align human-depleted reads to AF063224.1; mean depth across each SNP amplicon for each sample was calculated, excluding zero values, and then was normalized to total raw reads per million of the sample.

III. Experiment-specific protocols

III.A. Zika detection (Fig. 1c)

Nucleic acid amplification. Sample preparation was performed according to the method outlined in "General experimental procedures" II.A. "*CARMEN sample preparation*". For Zika virus detection (Fig. 1c, Extended Data Fig. 3b-e), recombinase polymerase amplification (RPA) was used. RPA reactions were performed using the Twist-Dx RT-RPA kit according to the manufacturer's instructions. Primer concentrations were 480 nM and $MgAc_2$ concentration was 17 mM. For amplification reactions involving RNA, Murine RNase

inhibitor (New England Biolabs) was used at a final concentration of 2 units per microliter. All RPA reactions were incubated at 41 °C for 20 minutes unless otherwise stated. RPA primer sequences are listed in the supplementary data. RPA reactions were diluted 1:10 in nuclease-free water prior to color coding.

Cas13 detection reactions. For Zika detection experiments (Fig. 1c), detection mixes were supplemented with $MgCl_2$ at a final concentration of 6 mM prior to droplet merging. For comparison between CARMEN and SHERLOCK (Extended Data Fig. 3b and c), a Biotek Cytation 5 plate reader was used for measuring fluorescence of the detection reaction. Fluorescence kinetics were monitored using a monochromator with excitation at 485 nm and emission at 520 nm with a reading every 5 minutes for up to 3 hours.

Color coding, emulsification, loading, imaging, and merging microwell arrays. Amplified samples and detection mixes (18 µl) were color coded using a subset of the 64 color code set. Color coded solutions were emulsified into droplets, pooled, and loaded onto a standard chip (see Section II.D and E). The chip was imaged with a 4× objective (Nikon, MRH00041) to identify color codes, droplet pairs were merged, and reporter fluorescence in each well was measured by fluorescence imaging at 3 hours. In this prototyping experiment, images were analyzed without background subtraction.

Analysis of Zika detection. Bootstrapping was performed to estimate the number of crRNA-Target pair replicates needed to reliably make a call. Sampling was done on two distributions: (1) crRNA-Target pairs expected to give a positive signal; (2) crRNA-control pairs expected to give a negative signal. A correct call was defined as the median of bootstrap samples from the positive distribution greater than the median of bootstrap samples in the negative distribution. 1000 bootstrap tests were performed for each sample size in the range of 1-15 samples. The fraction of correct calls was plotted as a function of bootstrap sample size.

III.B. Human-associated virus panel (Fig. 2)

Nucleic acid amplification. Sample preparation was performed according to the method outlined in "General experimental procedures" II.A. *"CARMEN sample preparation"*. For the Human-associated viral panel, amplification was performed using Q5 Hot Start polymerase (New England Biolabs) using primer pools (with 150 nM of each primer) in 20 µl reactions (see Section IV.A and Supplementary Data File 2 for a detailed description of primer pool design and construction). Each target ultramer was amplified with the primer pool containing its corresponding primer pair(s). The following thermal cycling conditions were used: (i) initial denaturation at 98 °C for 2 min; (ii) 45 cycles of 98 °C for 15 s, 50 °C for 30 s, and 72 °C for 30 s; (iii) final extension at 72 °C for 2 min. For synthetic targets, each target was amplified with its corresponding primer pool. For clinical samples, each sample was amplified with all pools. For clinical samples, amplification reactions were diluted and mixed into five "metapools" as follows: Pools 1-3, Pools 4-6, Pools 7-9, Pools 10-12, and Pools 13-15.

Cas13 detection reactions. Detection reactions were prepared as described in Section II.C. In the first round of testing, all 169 crRNAs were used. In the second round, two high-performing crRNAs were omitted with no discernable negative effects on panel performance. For clinical samples, all 169 crRNAs were used, along with the HCV2 crRNA.

Color coding, emulsification, loading, imaging, and merging microwell arrays. Amplified samples and detection mixes (18 µl) were color coded using a subset of the 1,050 color code set. Color coded solutions were emulsified into droplets, pooled, and loaded onto an mChip (see Section II.D and E). The chip was imaged with a 1× objective to identify color codes, droplet pairs were merged, and reporter fluorescence in each well was measured by fluorescence imaging at 1 hour and 3 hours (see Section II.E). Data were analyzed as described in Section II.F.

For the full panel testing (169 × 169), a single replicate of the equivalent experiment conducted in 96W plates would require ~300 plates and >1L of detection mix.

Threshold analysis of HV panel synthetic targets (Fig. 2c, Supplementary File 3). For each crRNA, a threshold for detection was set at 3 standard deviations above the background fluorescence. "Cross-reactivity" was defined as off-target reactivity above threshold. "Low-reactivity" was defined as no reactivity above threshold. "Selective" was defined as on-target reactivity above threshold and no cross-reactivity.

Analysis of patient sample testing with the 169-plex HV panel. To determine whether any crRNA in an experiment was uninterpretable due to signal above background in healthy control samples, the median signal across all crRNAs was calculated for each control sample. (Reactivity of the control samples across the 169-plex panel is expected to be very sparse, so the median value is a reliable measure of background signal.) Next, for each crRNA, a ratio was calculated of (numerator) the signal from the control sample with that crRNA and (denominator) the median for that control sample across all crRNAs. If any crRNA showed reactivity with a control sample that was >6x the median signal for that control sample, the crRNA was considered to be uninterpretable for that experiment. For each interpretable crRNA, the signal from each sample was divided by the median signal from the healthy control samples for that crRNA. Signal that was 6x above the median background signal was considered a positive result.

Commercial RT-PCR testing. RT-PCR testing for HCV and HIV was performed using the HCV TaqMan RT-PCR Kit and the HIV TaqMan RT-PCR Kit (both from Norgen Biosciences) according to the manufacturer's recommendations (with 5 µl of RNA as input). RT-PCR testing for Zika and dengue was performed using the RealStar® Dengue RT-PCR 3.0 kit and the RealStar® Zika Virus RT-PCR Kit (both kits were RUO versions, from Altona Diagnostics), according to the manufacturer's recommendations (with 10 µl of RNA as input). RT-PCR was performed using the Lyra Influenza A+B kit (Quidel) according to the manufacturer's instructions (with 2.5 µl of RNA as input).

III.C. Influenza A (Fig. 3)

Nucleic acid amplification. Sample preparation was performed according to the method outlined in "General experimental procedures" II.A. *"CARMEN sample preparation"*. For the Influenza subtyping panel, amplification was performed using Q5 Hot Start polymerase (New England Biolabs) using primer pools (with 150 nM of each primer) in 20 µl reactions. The following thermal cycling conditions were used: (i) initial denaturation at 98 °C for 2 min; (ii) 40 cycles of 98 °C for 15 s, 52 °C for 30 s, and 72 °C for 30 s; (iii) final extension at 72 °C for 2 min. For the experiments shown in Fig. 3d, H and N amplification reactions were diluted together. H reactions were diluted 1:10, and N were diluted 1:5, into nuclease-free water supplemented with 13.2 mM $MgCl_2$ prior to color coding.

Cas13 detection reactions. Detection reactions were prepared as described in Section II.C.

Color coding, emulsification, loading, imaging, and merging microwell arrays. Amplified samples and detection mixes (18 µl) were color coded using a subset of the 64 color code set. Color coded solutions were emulsified into droplets, pooled, and loaded onto a standard chip (see Section II.D and E). The chip was imaged with a 2× objective to identify color codes, droplet pairs were merged, and reporter fluorescence in each well was measured by fluorescence imaging at 1 or 3 hours (see Section II.E). Data were analyzed as described in Section II.F.

Analysis of patient sample testing with the influenza subtyping panel. The threshold for each crRNA may be set individually, as the reactivity of a crRNA is sequence-specific. For H-subtyping crRNA, the signal from each sample was divided by the median signal from the healthy control samples for that crRNA. Signal that was 6x above the median background signal was considered a positive result. The

N-subtyping crRNAs are less reactive, so a more sensitive threshold is necessary to accurately differentiate signal from background. For each N-subtyping crRNA, the median and standard deviation of the control samples was calculated, and a threshold of 7 standard deviations above the median was used to determine signal above background.

III.D. HIV DRMs (Fig. 4)

Nucleic acid amplification. Sample preparation was performed according to the method outlined in "General experimental procedures" II.A. "*CARMEN sample preparation*". For the HIV DRM panels, amplification was performed using Q5 Hot Start polymerase (New England Biolabs) using primer pools (with 150 nM of each primer) in 20 µl reactions. The following thermal cycling conditions were used: (i) initial denaturation at 98 °C for 2 min; (ii) 40 cycles of 98 °C for 15 s, 52 °C for 30 s, and 72 °C for 30 s; (iii) final extension at 72 °C for 2 min. For the experiments shown in Fig. 4, even and odd reactions were diluted together at 1:10 into nuclease-free water supplemented with 13.2 mM $MgCl_2$ prior to color coding.

Cas13 detection reactions. Detection reactions were prepared as described in Section II.C.

Color coding, emulsification, loading, imaging, and merging microwell arrays. Amplified samples and detection mixes (18 µl) were color coded using a subset of the 64 color code set. Color coded solutions were emulsified into droplets, pooled, and loaded onto a standard chip (see Section II.D and E). The chip was imaged with a 2× objective to identify color codes, droplet pairs were merged, and reporter fluorescence in each well was measured by fluorescence imaging at 30 minutes or 3 hours (see Section II.E). Data were analyzed as described in Section II.F.

Analysis of patient sample testing with the HIV RT DRM panel. In order for CARMEN to make a SNP call, the reactivity of one of the crRNAs (ancestral or derived) for that SNP must be above background. To filter out "no call" results, the sum of the ancestral and derived crRNAs for each SNP was divided by the sum of the minimum ancestral and minimum derived signal for those crRNAs. The "no call" threshold was 1.2x the sum of minimum values. For tests where a call could be made, the background-subtracted derived signal was divided by the background-subtracted ancestral signal. A threshold for each SNP was set based on the ratios from ancestral and derived synthetic sequences run in parallel with the patient samples, and the thresholds ranged from 1-3.

IV. Software and nucleic acid sequence design

IV.A. Human-associated virus panel design

Overview. A schematic overview of the human-associated virus panel sequence design strategy is shown in Extended Data Fig. 5h. Briefly, the design pipeline consisted of viral genomes segment alignment, PCR amplicon selection, followed by crRNA design that accounts for cross-reactivity. Finally, PCR primers were pooled by genus. All sequences are in Supplementary Data File 2.

Viral genome segment alignment. Viral genome neighbors were downloaded from NCBI(*2*). Each segment of each viral species was aligned using mafft v7.31[33] with the following parameters: --retree 1 --preservecase. Alignments were curated to remove sequences that were assigned the wrong species, reverse-complemented, or came from the wrong genome segment. A the aligned genome segments can be found at the following link: https://storage.googleapis.com/sabeti-public/carmen_design/hav10_fft1_alignments.tar.gz.

PCR amplicon selection. Potential PCR binding sites were identified by using ADAPT with a window size of 20 nucleotides, and a coverage requirement of 90% of the sequences in the alignment (Metsky *et al. in prep*). Potential pairs of primer binding sites within a distance of 70 to 200 nucleotides were selected. These sets of potential primer pairs were input into primer3 v2.4.0[28] to see if suitable PCR primers could be designed for amplification. Primer3 was run using the following parameters: PRIMER_TASK=generic, PRIMER_EXPLAIN_FLAG=1, PRIMER_MIN_SIZE=15, PRIMER_OPT_SIZE=18, PRIMER_MAX_SIZE=20, PRIMER_MIN_GC=30.0, PRIMER_MAX_GC=70.0, PRIMER_MAX_Ns_ACCEPTED=0, PRIMER_MIN_TM=52.0, PRIMER_OPT_TM=54.0, PRIMER_MAX_TM=56.0, PRIMER_MAX_DIFF_TM=1.5, PRIMER_MAX_HAIRPIN_TH=40.0, PRIMER_MAX_SELF_END_TH=40.0, PRIMER_MAX_SELF_ANY_TH=40.0, PRIMER_PRODUCT_SIZE_RANGE=70-200. A list of potential amplicons was generated by parsing the primer3 output file, filtering to ensure that the maximum difference in melting temperature between any pair of forward and reverse primers was less than 4 °C (so that all primers in the pool would have similar PCR efficiency). This list of potential amplicons was then scored based on the average pairwise penalty between all pairs of forward and reverse primers in the design, as measured by primer3. The amplicon with the highest score from each species was chosen for crRNA design (see Supplementary Data File 2 for primer and amplicon sequences).

crRNA design. We used a software package called ADAPT (Metsky et al. in prep), which implements an algorithm to design crRNAs, such that the number of them approximates the minimum number of crRNAs that bind to 90% of the sequences within a 40 nt window of each amplicon alignment, allowing for up to one mismatch between each crRNA and target sequence, and allowing for G-U pairing. These crRNA sets are designed in silico by the algorithm to avoid cross-reactivity at the family level, requiring 3 or more mismatches for >99% of sequences in the other species within the same family, allowing for G-U pairing. This stringent threshold was chosen to ensure high specificity for the human-associated virus assay. For closely related viral genuses (enterovirus, and poxvirus), the algorithm selected regions where the majority consensus sequence for each species differed and only considered crRNAs in windows where there was sufficient sequence divergence at the majority consensus level (see Supplementary Data File 2 for crRNA sequences).

Primer pooling. We designed primers (as described above) for a set of 169 species that have at least one segment with ≥10 sequences in the downloaded data, hereafter referred to as the human-associated virus panel 10 version 1 or hav10-v1. Due to limitations of multiplexed PCR, the 210 primer pairs that we designed for the 169 hav10 species in the version 1 design were split into 15 primer pools, described in more detail below.

Conserved primer pool. We selected 14 conserved species as a pilot experiment to test our primer design algorithm and pooling strategy. Species are listed in Supplementary Data File 2. These species were combined into a single "conserved" primer pool at 150 nM final concentration. This is Pool 1, as shown in Fig. 2C.

Diverse primer pool. 164 of the 169 hav10 species have designs with 3 or fewer primer pairs (total of 187 primer sequences required to cover these 164 species: 145 have 1 primer pair, 15 have 2 primer pairs, and 4 have 3 primer pairs). There were four species that required more than three primer pairs: Lymphocytic Choriomeningitis Virus (LCMV, 7 primer pairs), Norovirus (4 primer pairs), Betapapillomavirus 2 (6 primer pairs), and Candiru Phlebovirus (6 primer pairs). These four species were combined into a single "diverse" primer pool at 150 nM final concentration. This is Pool 2, as shown in Fig. 2C.

Degenerate primer pool. For 167 of the 169 hav10 species, it was possible to design primer sets using ADAPT/primer3 that cover >90% of the genomes in the database with fewer than 10 primer pairs. However, for two species (Simian Immunodeficiency Virus and Sapporo virus) it was not possible to identify sufficiently conserved pairs of primer binding sites using our computational design strategy. Instead, we designed primers with several degenerate bases to capture the extensive sequence diversity, and manually identified amplicons. These two primer pairs were used in a "degenerate" primer pool at 600 nM final concentration. This is Pool 3, as shown in Fig. 2C.

Remaining primer pools. For the remaining 149 hav10 species, we pooled primers by genus, such that each pool contained species from 1-3 viral genuses (see Supplementary Data File 2 for details). The primers

for one species in pool 4 (Torque teno Leptonychotes weddellii virus-1) contain some degenerate bases, and were designed manually. These primers were used at 150 nM final concentration.

Coronavirus primer pool. primers used in the coronavirus panel are indicated in Supplementary Data File 2. These primers were used at 150 nM final concentration.

Version one design analysis. In the analysis of version one performance, it was discovered that crRNA 136 had inadvertently been designed against Target 128. Both crRNA 128 and crRNA 136 selectively react with Target 128, and were thus counted as "Selective" crRNAs. To computationally analyze the expected version one design performance, spacer target sequences and primers were aligned using bwa 0.7.17-r1188[32] against the majority consensus sequences of each of the 169 viral genomes. Alignments with insertions or deletions were not permitted. Primers and crRNAs activity were scored using the alignments output by bwa. The score for both primers and crRNAs was the number of matching bases between the crRNA and target sequence, except for crRNA activity the score also counted crRNA-target pairs of A-G and C-T to include G-U pairing. Score cutoffs were 17 for primers and 27 for crRNAs. This yielded a 169x169 predicted reactivity matrix for the primers, and another matrix for the crRNAs. This matrix was summed to calculate the expected number of targets that each primer or crRNA would react with. A score of 0 was categorized as low activity, a score of 1 as perfect activity, and a score >1 as cross-reactivity.

Version two redesign. After testing the hav10-v1 design, 3 amplicons were redesigned: Orthohepesvirus A, Rhinovirus A, and Rhinovirus B. The newly designed primers were re-pooled to create pools 8v2 and 12v2, and new crRNA sequences were designed to target these amplicons. Based on the results of the hav10-v1 testing we redesigned crRNAs within the existing v1 amplicons for 14 species (see Supplementary Data File 2 for details).

IV.B. Influenza A design

Primer design. N (neuraminidase) primers were based on the majority consensus sequence for each subtype (9 primer pairs) in a single pool. We used ADAPT to design H (hemagglutinin) primers covering at least 95% of the sequences within each subtype. In total, there were 45 primers (15 forward primers, 30 reverse primers) in a single pool. See Supplementary Data File 2 for details.

crRNA design. Sets consisting of a small number (1-5) of crRNA sequences were designed to selectively target individual H or N subtypes using ADAPT (Metsky *et al. in prep*). We improved our design approach throughout the process by incorporating new features into each round of design. In the first round of design, we only designed H crRNAs, and required that all crRNAs could hybridize with 90% of all sequences, allowing for up to 1 mismatch. crRNAs in a set could be positioned anywhere in the amplicon. In the second round of design, we designed crRNAs for both H and N and restricted the positions of crRNAs within a set (to within a 91 nt window for H, and 35 nt window for N) as some positions within the amplicon were more conserved between subtypes than others. As in round 1, in round 2 we required that all crRNAs could hybridize with 90% of all sequences, allowing for up to 1 mismatch. In addition, we weighted the coverage of our designs towards more recent years by using an exponential decay parameter for sequences older than 2017. In the third round, we used a differential design approach in which all crRNAs were required to have at least 3 mismatches against at least 99% of sequences within any other subtype. In the fourth round, we accounted for G-U pairing in hybridization, and raised the target threshold to 95% of sequences in each subtype, allowing for up to 1 mismatch. Each round of designs was tested experimentally, and high-performing crRNAs between designs were used in combination. H required 4 rounds of design, while N only required 2 (rounds 2 and 3). Oligonucleotide sequences are listed in Supplementary Data File 2.

IV.C. HIV DRM panel design

Primer design. We used a primer pooling strategy in which primer pairs were divided into overlapping "odd" and "even" primer pools based on the locations of DRMs within the reverse transcriptase and integrase genes[34]. This allowed for all mutations to be contained in at least one amplicon, without creating any issues during amplification. Primer sequences were designed using primer3 v2.4.0 with the following parameters: PRIMER_PRODUCT_OPT_SIZE=150, PRIMER_MAX_GC=70, PRIMER_MIN_GC=30, PRIMER_OPT_GC_PERCENT=50, PRIMER_MIN_TM=55, PRIMER_MAX_TM=60, PRIMER_DNA_CONC=150, PRIMER_OPT_SIZE=20, PRIMER_MIN_SIZE=16, PRIMER_MAX_SIZE=29. Amplicon lengths ranged between 150 and 250 nucleotides. All primer sequences are in Supplementary Data File 2.

crRNA design. Pairs of crRNAs were designed for HIV DRM identification using three different strategies: mutation on position 3 and synthetic mismatch on position 5, DRM codon on positions 3-5 and synthetic mismatch on position 6, and DRM codon on positions 4-6 with synthetic mismatch at position 3. Sequences were designed based on the HIV subtype B consensus sequence, using the most-commonly used codons for each respective amino acid in the Stanford HIV Drug Resistance Database[35]. All designs were experimentally tested, and the best-performing design was chosen for the final panel.

V. Hardware development and construction

V.A. Microwell array chip design and fabrication

Microwell array design. Microwell dimensions were optimized by empirical testing to balance droplet loading speed (faster with larger wells) and droplet-droplet closeness inside a microwell (better merging with smaller wells). For droplets made from PCR amplification reactions or Cas13 detection mix, the optimal microwell geometry was achieved by joining two circles with diameters of 158 µm and an overlap of 10% (Extended Data Fig. 1c). The microwells were designed with a minimum distance of 37 µm between each well to facilitate consistent chip fabrication without PDMS tearing (see Microwell chip fabrication, below). Standard chips have a total microwell array that is 6.0 × 5.5 cm (51,496 microwells); the loading slot partially obscures the microwell array, reducing the functional array size to 6.0 × ~4.5 cm (~42,400 microwells) (Extended Data Fig. 1d). mChips have a microwell array that is 12 × 9.1 cm, bearing 177,840 microwells (Extended Data Fig. 5a). The mChip microwell array is surrounded by a 0.1-0.3 cm border of unpatterned PDMS to facilitate a robust seal around the edge of the chip. The total mChip dimensions were designed to maximize the number of wells that can be imaged on the area of a standard microscope stage (16 × 11 cm opening, Bio Precision LM Motorized Stage, Ludl Electronics), while still allowing the chip to be fabricated using standard silicon wafers (15 cm diameter) (Extended Data Fig. 5b).

Microwell chip fabrication. Polydimethylsiloxane (PDMS) chips were fabricated according to standard hard and soft lithography practices using acrylic molds to achieve consistent chip dimensions; the fabrication of standard size chips has been described previously[8]. For mChips, 150 mm wafers (WaferNet, Inc., #S64801) were washed on a spin coater (Model WS-650MZ-23NPP, Laurell Technologies) at 2500 rpm, once with acetone and once with isopropanol. Photoresist (SU-8 2050, MicroChem) was spin-coated onto each wafer in a two-step process: (1) 30 seconds, 500 rpm, acceleration 30; (2) 59 seconds, 1285 rpm, acceleration 50. Wafers were baked at 65 °C for 5 minutes and, subsequently, at 95 °C for 18 minutes. After a 1 minute cooling period, the coated wafer was placed under the appropriate photomask and irradiated (5 × 3 seconds, 350 W, Model 200, OAI). The wafer was baked again at 65 °C for 3 minutes and 95 °C for 9 minutes. After 1 minute of cooling, the wafer was incubated for 5 minutes under SU-8 developer. The developer was removed by spinning at 2500 rpm, and acetone and isopropanol washes were applied directly to the spinning wafer to remove excess developer and photoresist. Each wafer was characterized

by visual inspection under a light microscope and profilometry to measure feature dimensions (Contour GT, Bruker). Wafers were placed inside acrylic molds and secured with magnets (Extended Data Fig. 5b). To fabricate chips from the molds, PDMS was mixed (Thinky planetary vacuum mixer, ARV-310) and poured into the mold, and the entire mold was placed under house vacuum for 3-5 minutes. The mold was closed with an acrylic lid to achieve uniform chip thickness, and the chips were baked for at least 2 hours. After the chip was removed from the mold, the surface of the chip bearing the microwell array and the sides (but not the back of the chip opposite the microwell array) were coated with 1.5 µm Parylene C (Paratronix/MicroChem, Westborough, MA). Chips were stored in plastic bags at room temperature until use.

Acrylic device fabrication (molds and loaders). Molds[8] and loaders[36] for standard chip production and handling were constructed as described previously. Similar methods were used to construct molds and loaders for mChip (Extended Data Fig. 5b and d). Briefly, 12" × 12" cast acrylic sheets (¼" or 1/8", clear or black) were purchased from Amazon (Small Parts, #B004N1JLI4). Mold and loader designs were created in AutoCAD (AutoDesk), and parts were cut using an Epilog Fusion M2 laser cutter (60 W). Acrylic parts were fused together by wetting with dichloromethane (Sigma Aldrich). N42 Neodymium disc magnets (Applied Magnets, Inc., Plano, TX) were added to devices with epoxy (Loctite, Metal/Concrete). Cap screws (M4 × 25), nuts (M4), and washers (M4) were purchased from Thorlabs.

V.B. Color code design, construction, and characterization

Color code design. Color codes served as optical unique solution identifiers for each reagent (e.g. detection mix or amplified sample) that was emulsified into droplets. The original 64 color code set was made from ratios of 3 fluorescent dyes, such that the total concentration of the three dyes ([dye 1] + [dye 2] + [dye 3]) was constant and served as an internal control to normalize for variation in illumination across the field of view or at different locations on the chip[8]. The working total dye concentration for the 64 color code set was 1-5 µM, as described previously[8]. The 1,050 color codes were designed by (1) increasing the total working concentration of the 3 fluorescent dyes to 20 µM, such that 210 color codes could be faithfully identified in 3-color space (Extended Data Fig. 4a and b), and (2) adding a fourth fluorescent dye at one of five concentrations (0, 3, 7, 12 or 20 µM) to multiply the 210 codes by five (Extended Data Fig. 4a). In this design, each of the 4 dye intensities is normalized to the sum of the first 3 fluorescent dyes.

Color code construction. The standard 64 color code set (50 µM stock concentration; 1-5 µM working concentration) was constructed as previously described[8] (Supplementary Data File 1). The 210 color codes (400 µM stock concentration; 20 µM working concentration, see Supplementary Data File 1 for ratios) were constructed using similar methods, as follows. Alexa Fluor 647 (AF647), Alexa Fluor 594 (AF594), Alexa Fluor 555 (AF555), and Alexa Fluor 405 NHS ester (AF405-NHS) (Thermo Fisher) were diluted to 25 mM in DMSO (Sigma). Since the molar masses of these dyes is proprietary, the following approximate masses provided by the manufacturer were used for calculations: AF647: 1135 g/mol; AF594: 1026 g/mol; AF555: 1135 g/mol; AF405-NHS: 1028 g/mol. Dye stocks in dimethyl sulfoxide (DMSO) were further diluted to 400 µM in DNase/RNase-free water (Life Technologies). Alexa Fluor 405 NHS ester was incubated at room temperature for one hour to allow hydrolysis of the NHS ester and generate Alexa Fluor 405 (AF405). Custom MATLAB scripts were used to calculate the dye volumes to combine to evenly distribute 210 color codes across the 3-color space (Supplementary Data File 1). 3-color dye combinations (made from AF647, AF594, and AF555) were constructed in 96 well plates (Eppendorf) using a Janus Mini liquid handler (Perkin Elmer). To construct 1,050 color codes, AF405 was manually diluted to five concentrations (0, 60, 140, 240, and 400 µM), and each concentration was arrayed across a 96 well plate. Each of the 210 color codes (10 µl) and AF405 (10 µl) were combined and mixed in a fresh 96 well plate using a Bravo liquid handler (Agilent). The final stock concentration of the sum of AF647, AF594, and AF555 was 200 µM; the final concentrations of AF405 were 0, 30, 70, 120, and 200 µM. Stocks were diluted 1:10 into amplified samples or detection mixes for use.

Characterization of 1,050 color code set. Each color code was diluted 1:10 in LB broth (a medium that yields droplets of similar size to droplets made from PCR products and detection reagents) to a final total 3-dye concentration of 20 µM. Each solution was emulsified into droplets as described in Section II.D., above. The 1,050 color code set was characterized in 3-color space and along the 4th color dimension, as described below.

Characterization in 3-color space. The fidelity of the color code strategy in 3-color space was measured as described previously[8]. Each color code in 3-color space was assigned to one of three chips. Assignments were made to maximize the separation between the color codes on any chip, and each chip received 1/3 of the color codes (70 total) (Extended Data Fig. 4b and c). Droplets from color codes assigned to Chip 1 (70 3-color codes × 5 UV concentrations = 350 droplet emulsions) were pooled (see Section II.D.) and loaded onto a standard chip (see Section II.E.). Chips 2 and 3 were prepared in a similar manner. The chips were imaged (see Section II.E.; note that no merging was performed in color code characterization experiments), and each droplet was computationally assigned to a color code cluster. The experimental results from Chips 1, 2, and 3 served as "ground truth" assignments. The data from Chips 1, 2, and 3 were then computationally combined, effectively increasing the density of color code clusters in 3-color space, and the droplets were reassigned to color code clusters in this more crowded 3-color space (Extended Data Fig. 4b and c). Finally, a sliding distance filter was applied to remove droplets at the edges of clusters or in between clusters, and the droplets were reassigned to color code clusters (Extended Data Fig. 4b and f). The sliding distance filter refers to a radius around each cluster centroid that is used to remove droplets that fall in the space between clusters (Extended Data Fig. 4f). The radius may be larger (to include more droplets) or smaller (to more stringently filter out droplets). New assignments were compared to "ground truth" assignments to measure the percent of droplets that would be misclassified if the color codes were not separated over three chips (Extended Data Fig. 4d and e). In the work presented here, the radius of the sliding distance filter was set to achieve at least 99.5% correct classification in the test data set, corresponding to the removal of 6% of droplets.

Characterization along the 4th-color dimension. The five concentrations of the 4th fluorescent dye were divided between two chips (Chip 1: 0, 7, 20 µM; Chip 2: 3, 12 µM) (Extended Data Fig. 4g). Droplets from dye intensities assigned to Chip 1 (3 UV intensities × 210 color codes = 620 emulsions) were pooled (see Section II.D.) and loaded onto a standard chip (see Section II.E.). Chip 2 was prepared in a similar manner but with fewer pooled emulsions (2 UV intensities × 210 color codes = 420 emulsions). The chips were imaged (see Section II.E.; note that no merging was performed in color code characterization experiments), and each droplet was computationally assigned to a UV intensity bin. The experimental results from Chips 1 and 2 served as "ground truth" assignments. The data from Chips 1 and 2 were then computationally combined, effectively increasing the density of UV intensity bins along the 4th-color dimension, and the droplets were reassigned to UV intensity bins in this more crowded space (Extended Data Fig. 4g). Finally, a sliding distance filter was applied to remove droplets at the edges of intensity bins or in between intensity bins, and the droplets were reassigned to UV intensity bins (Extended Data Fig. 4g). New assignments were compared to "ground truth" assignments to measure the percent of droplets that would be misclassified if the UV intensities were not separated over three chips (Extended Data Fig. 4g). As classification in the 4th-color dimension is sufficiently high (>99.5% accurate) without filtering, no filtering in the 4th-color dimension was applied to the experimental data.

Reporting summary

Further information on research design is available in the Nature Research Reporting Summary linked to this paper.

Data Availability

The CARMEN datasets generated during and/or analysed during the current study are available from the corresponding authors on reasonable request. Fluorescence values for rounds 1 and 2 of the HV panel testing and patient sample testing are included in Supplementary Data Files 3-7. Viral sequencing data has been posted in a public repository (PRJNA623215).

Code Availability

The code used for CARMEN data analysis is available on GitHub at https://github.com/blaineylab/kChip/tree/kchip_UV and https://github.com/blaineylab/kChip/tree/kchip_clustering.

31. Matranga, C. B. *et al*. Enhanced methods for unbiased deep sequencing of Lassa and Ebola RNA viruses from clinical and biological samples. *Genome Biol*. **15**, 519 (2014).
32. H. Li, Aligning sequence reads, clone sequences and assembly contigs with BWA-MEM (2013), (available at http://arxiv.org/abs/1303.3997).
33. K. Katoh, D. M. Standley, MAFFT multiple sequence alignment software version 7: improvements in performance and usability. *Mol. Biol. Evol*. **30**, 772–780 (2013).
34. J. Quick *et al*., Multiplex PCR method for MinION and Illumina sequencing of Zika and other virus genomes directly from clinical samples. *Nat. Protoc*. **12**, 1261–1276 (2017).
35. S.-Y. Rhee *et al*., Human immunodeficiency virus reverse transcriptase and protease sequence database. *Nucleic Acids Res*. **31**, 298–303 (2003).
36. J. Kehe *et al*., Massively parallel screening of synthetic microbial communities. *Proc. Natl. Acad. Sci. U. S. A*. **116**, 12804-12809 (2019).

Acknowledgements We are grateful to J. Gootenberg, O. Abudayyeh, E. Spady, and Sabeti and Blainey lab members for discussions and thoughtful manuscript feedback, and Boca Biolistics for support with patient samples. Funding was provided by: Defense Advanced Research Projects Agency (DARPA) grant D18AC00006, the Howard Hughes Medical Institute, the Koch Institute for Integrative Cancer Research Bridge Project, an MIT Deshpande Center Innovation Award, the Merkin Institute for Transformative Technologies in Healthcare, and a Burroughs Wellcome Fund CASI Award (to PCB). CMA was supported by NIH grant F32CA236425. The views, opinions, and/or findings expressed should not be interpreted as representing the official views or policies of the Department of Defense, NIH, or the U.S. government. This study has been approved for public release; distribution is unlimited.

Author contributions CMA and CM contributed equally to this work and are listed in alphabetical order. GT and CAF contributed equally to this work. PCB and PCS contributed equally to this work and are listed in alphabetical order. CM, CMA, CAF, GT, and JK conducted proof-of-concept and exploratory experiments. CMA, JK, AK, and GT designed the color code expansion. CMA designed and characterized hardware and reagents for massive multiplexing (color codes and mChip), imaging methods, and accompanying data analysis. HCM wrote the software for crRNA design. CM designed the human-associated viral panel and influenza subtyping panel with data from HCM. CM and DKY designed the HIV DRM identification panels. CM and CMA designed experiments, supervised by PCB and PCS. CM, CMA, CAF, DKY, and GT prototyped the influenza subtyping and HIV DRM identification panels. CM, CMA, CAF, CKB, TN, TSKT, and AC tested the human-associated viral, influenza subtyping, and HIV DRM panels. CAF performed sequencing experiments; HCM, SHY, and CAF performed data analysis. JRB and VGD provided influenza samples. DTH, PCB, and PCS supervised the research and provided feedback on experimental direction. CM and CMA wrote the paper, with contributions from JK, DKY, GT, PCB, and PCS. All authors provided feedback and edited the text.

Competing interests CMA, CM, GT, CAF, HM, JK, DTH, PCB, and PCS are co-inventors on patent applications filed by the Broad Institute relating to work in this study. Additional related applications for intellectual property have been filed by the Broad Institute. PCS is a co-founder of and consultant to Sherlock Biosciences and Board Member of Danaher Corporation, and holds equity in both companies. DTH is also a co-founder of Sherlock Biosciences. In addition, PCB is a consultant to and equity holder in companies in the microfluidics and life sciences industries including 10X Genomics, GALT, Celsius Therapeutics, and Next Generation Diagnostics.

Additional information
Supplementary information is available for this paper at https://doi.org/10.1038/s41586-020-2279-8.
Correspondence and requests for materials should be addressed to C.M., P.C.B., C.M. or P.C.B.
Peer review information *Nature* thanks Emily Crawford, Daniel Chertow, Gregory Storch and Jeff Wang for their contribution to the peer review of this work.
Reprints and permissions information is available at http://www.nature.com/reprints.

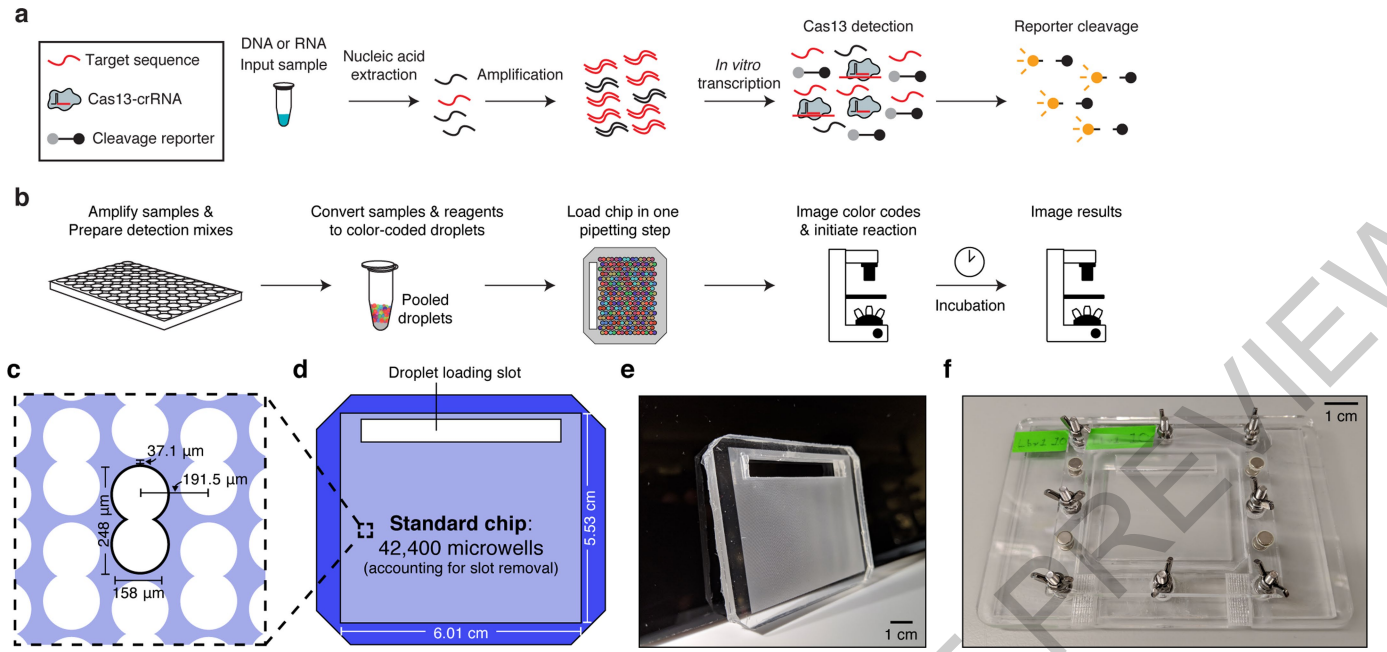

Extended Data Fig. 1 | The CARMEN workflow at the molecular and macroscopic scale. a, Detailed molecular schematic of nucleic acid detection in CARMEN-Cas13. After amplification (with optional reverse transcription), detection is performed with Cas13, using *in vitro* transcription to convert amplified DNA into RNA. The resulting RNA is detected with exquisite sequence specificity by Cas13-crRNA complexes, and collateral cleavage activity of Cas13 produces a signal using a cleavage reporter RNA. **b**, Overview of the CARMEN workflow. Amplified samples and detection mixes are color coded, emulsified, and pooled into one tube. In a single pipetting step, the pool of droplets is loaded onto a chip where the droplets self-organize into pairs. Fluorescence microscopy is used to read the color code of each droplet, mapping the position of each sample and detection mix in the chip, and droplets in each well are merged, initiating all reactions across the chip nearly instantaneously. After incubation, the reaction result for each well is read using fluorescence microscopy and mapped back to the color codes of the sample and/or detection mix in each well. **c**, Microwell design optimized for droplets made from PCR products or detection mixes. **d**, Dimensions and layout of a standard chip. Light blue is the area covered by the microwell array. **e**, Photograph of a standard chip. **f**, Photograph of a standard chip sealed inside an acrylic loader, ready for imaging.

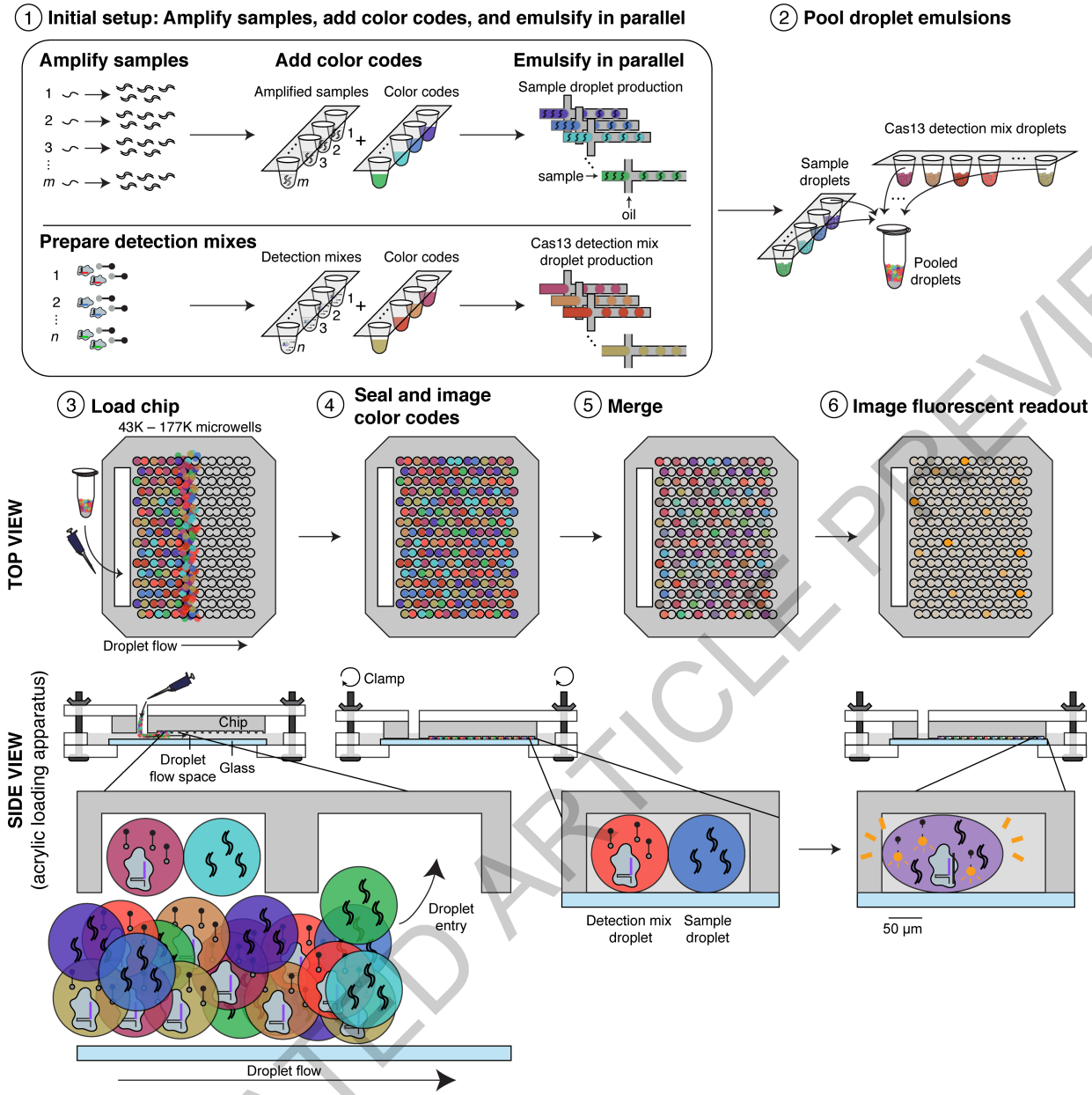

Extended Data Fig. 2 | Detailed schematic of loader and chip function in CARMEN. (Step 1) Samples are amplified, color coded, and emulsified. In parallel, detection mixes are assembled, color coded, and emulsified. (Step 2) Droplets from each emulsion are pooled into a single tube and mixed by pipetting. The pooling step is rapid to minimize small molecule exchange between droplets (see Supplementary Discussion IV). (Step 3) The droplets are loaded into the chip in a single pipetting step. SIDE VIEW: The droplets are deposited through the loading slot into the flow space between the chip and glass. Tilting the loader moves the pool of droplets around the flow space, allowing the droplets to float up into the microwells. (Step 4) The chip is clamped against glass, isolating the contents of each microwell, and imaged by fluorescence microscopy to identify the color code and position of each droplet. (Step 5) Droplets are merged, initiating the detection reaction. (Step 6) The detection reactions in each microwell are monitored over time (a few minutes - 3 hours) by fluorescence microscopy.

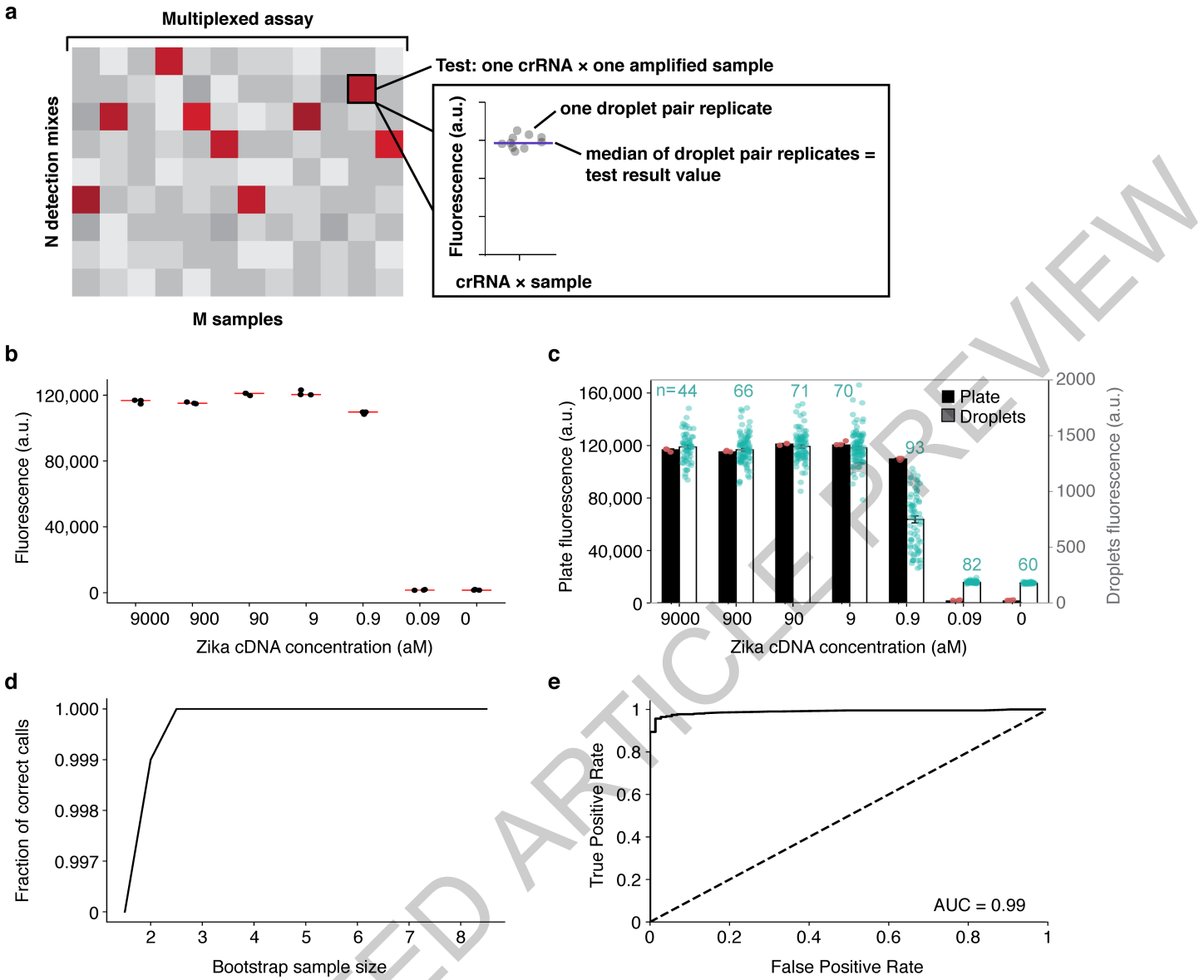

Extended Data Fig. 3 | CARMEN multiplexed detection nomenclature and detection of Zika sequences. a, Assay, test, and droplet pair replicate nomenclature. Each multiplexed assay consists of a matrix of tests, where the dimensions of the matrix are M samples × N detection mixes. Each test is the result of one sample being evaluated by one detection mix, where the result of the test is the median value of a set of replicate droplet pairs in the microwell array. **b**, Plate reader data for SHERLOCK detection of synthetic Zika sequences at 3 h (n=3 replicates). **c**, Comparison of plate reader and droplets (Fig. 1c) data. Replicates: n=3 for plate reader data. Numbers of replicates for droplets data are indicated in teal. Error bars represent standard error. **d**, Bootstrap analysis of Zika detection in droplets. **e**, Receiver operating characteristic (ROC) curve for Zika detection in droplets. AUC: area under the curve.

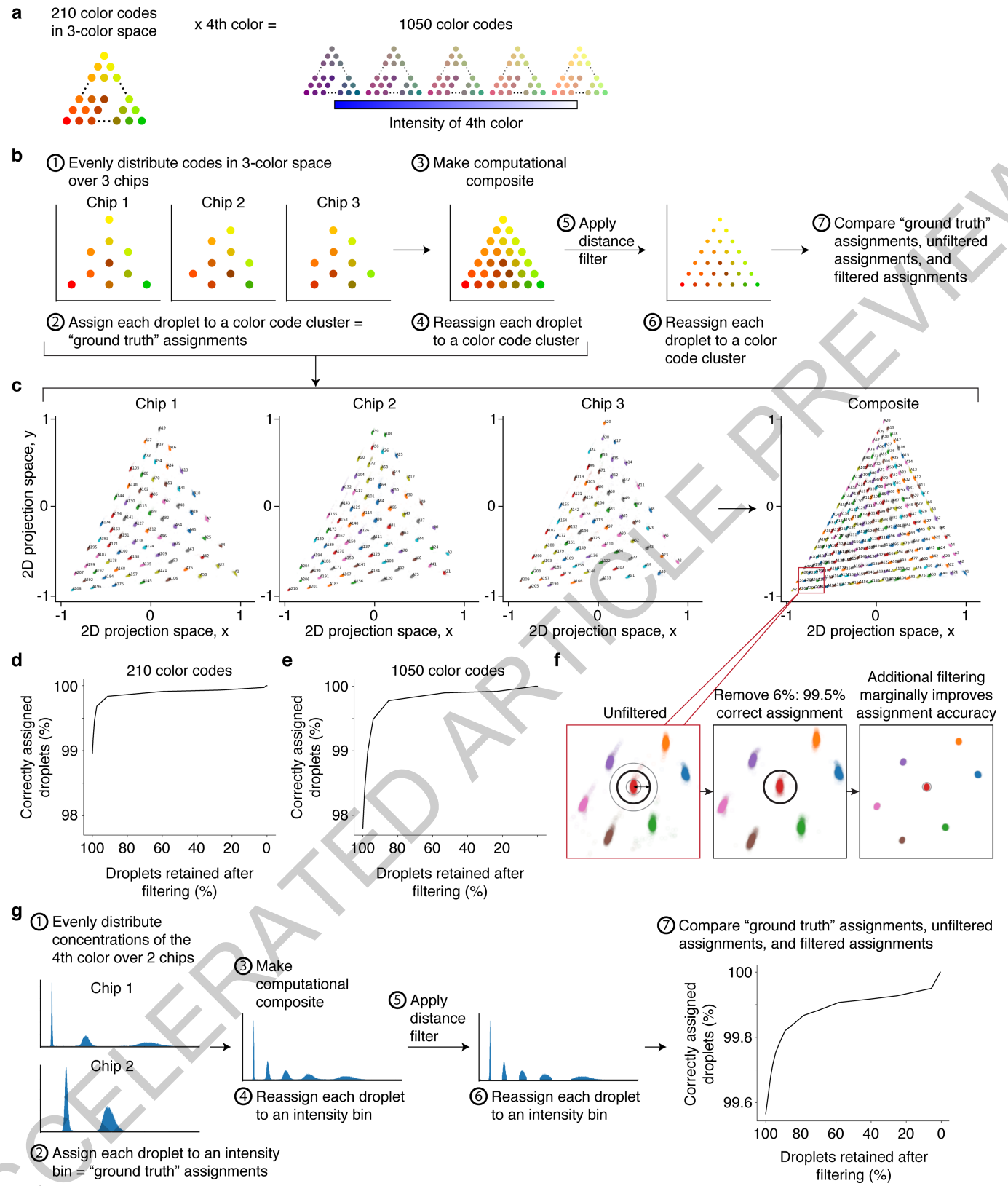

Extended Data Fig. 4 | Design and characterization of 1,050 color codes. **a**, Design of 1,050 color codes. **b**, Schematic for characterization of 210 color codes and the 3-color dimension of 1,050 color codes. **c**, Raw data from characterization of 210 color codes. **d**, Performance of 210 color codes in 3-color space. **e**, Performance of 1,050 color codes in 3-color space. **f**, Illustration of the sliding distance filter (circle) in 3-color space. **g**, Characterization schematic and performance of 1,050 color codes in the 4th color dimension.

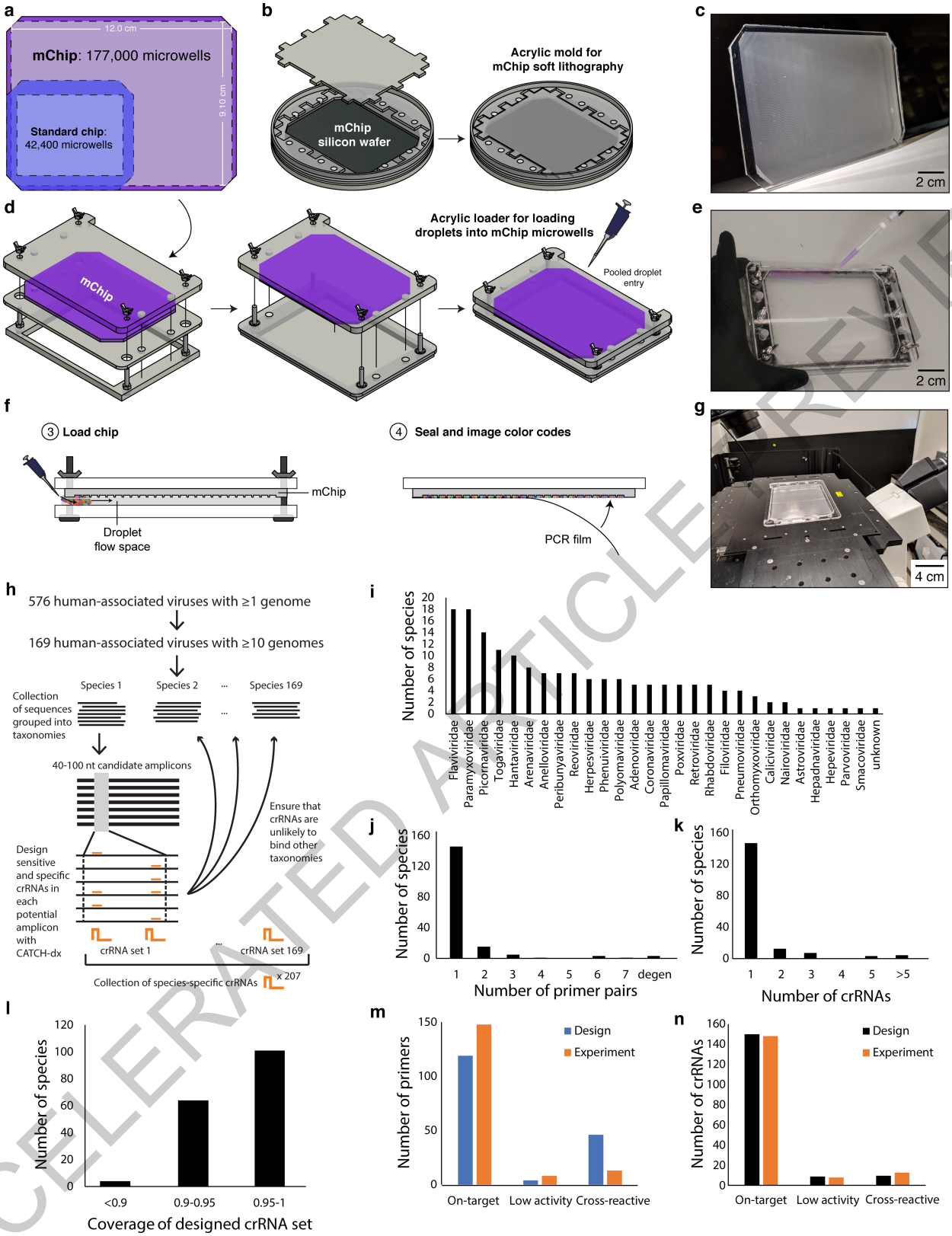

Extended Data Fig. 5 | See next page for caption.

Extended Data Fig. 5 | mChip and human-associated virus (HV) panel design schematic and statistics. a, Dimensions and layout of mChip, compared to a standard chip. Light purple is the area covered by the microwell array. **b**, AutoCAD rendering of acrylic molds used for mChip fabrication. **c**, Photograph of an mChip. **d**, (left) AutoCAD rendering of each part of the mChip loader; (middle) AutoCAD rendering of the set-up of an mChip loader; (right) AutoCAD rendering of an mChip in a loader, ready to be loaded. **e**, Photograph of an mChip being loaded. **f**, Loading and sealing mChip, corresponding to steps in Extended Data Fig. 2: (Step 3) mChip loading: Droplets are deposited at the edge of the chip into the flow space between the chip and the acrylic loader. Tilting the loader moves the pool of droplets around the flow space, allowing the droplets to float up into the microwells. (Step 4) The chip and loader lid are removed from the base and sealed against PCR film. No glass is used to seal the mChip. The sealed mChip, suspended from the acrylic loader lid, can be placed directly onto the microscope for imaging. **g**, Photograph of an mChip sealed and ready to be imaged. **h**, Human-associated viral panel design. At the time we designed the panel (Oct 2018), there were 576 human-associated viral species with at least 1 genome neighbor in NCBI, and 169 with ≥10 genome neighbors. We aligned genomes by segment and analyzed the sequence diversity using ADAPT to determine optimal primer and crRNA binding sites (see Methods for details). **i**, Number of species in each family in the human-associated virus panel design. **j**, Number of primer pairs required to capture at least 90% of the sequence diversity within each species. Two species required the use of primer pairs containing degenerate bases. **k**, Number of crRNAs required to capture at least 90% of the sequence diversity within each species. **l**, The fraction of sequences within each species covered by each designed crRNA set; we were able to design small crRNA sets with 90% or greater coverage for 164 of the 169 species. To compare expected and observed performance for the HV panel, **m**, primers and **n**, crRNAs were classified into on-target, low activity, or cross-reactive by sequence analysis (blue or black) or based on experimental data (orange).

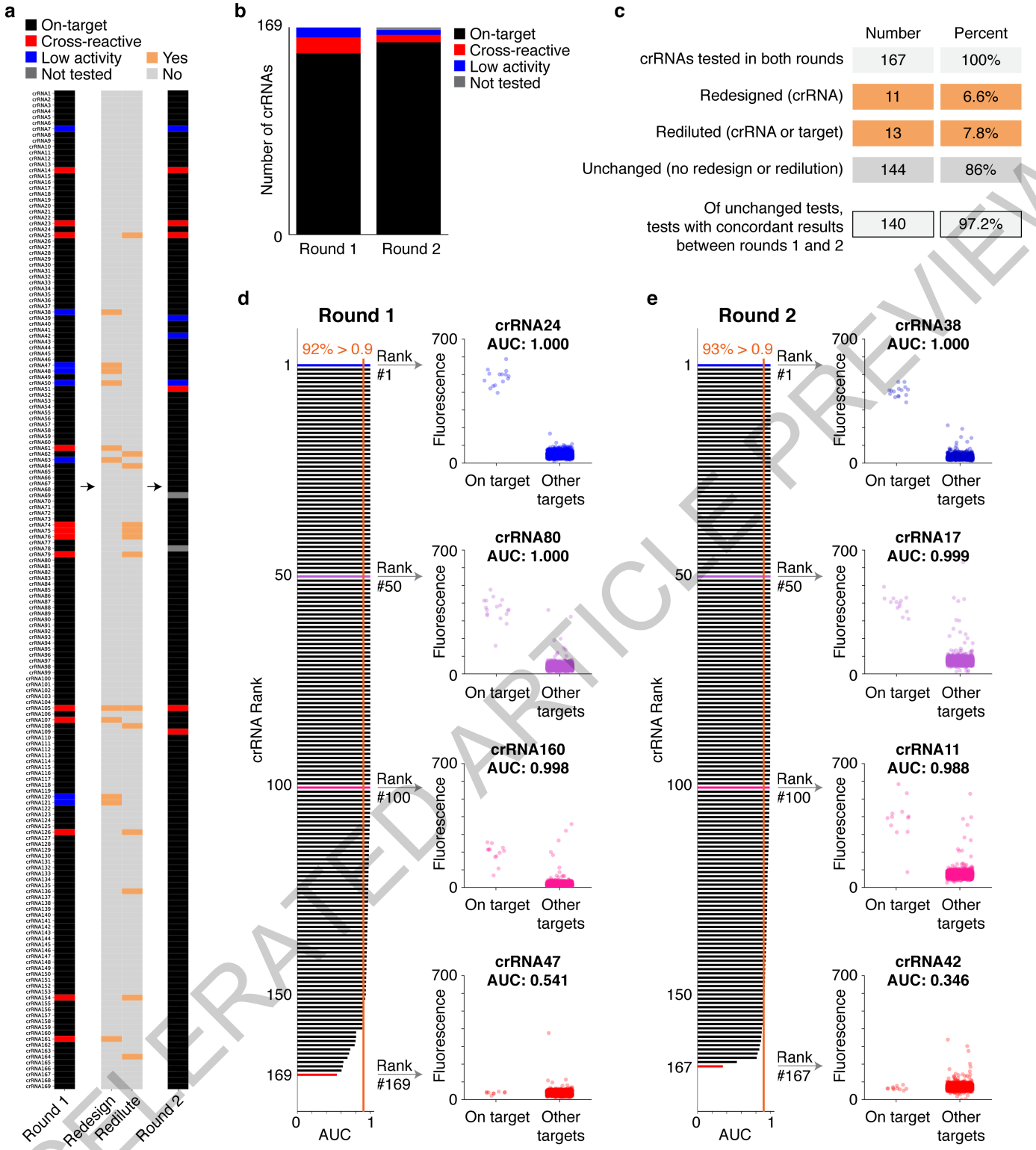

Extended Data Fig. 6 | crRNA performance during human-associated virus panel testing. a, Individual guide performance for rounds 1 and 2. Redesign and redilution between rounds of testing are indicated between the data from rounds 1 and 2. "On-target": reactivity above threshold for intended target only. "Cross-reactive": off-target reactivity above threshold. "Low activity": no reactivity above threshold. **b**, Summary bar graph of crRNA performance in rounds 1 and 2. **c**, Summary table of redesign, redilution, and concordance between rounds 1 and 2 for unchanged tests. **d**, Round 1 and **e**, round 2 ranked areas under the curve (AUC) for receiver operating characteristics for on-target vs off-target reactivity in round 1 of testing. Representative on-target and off-target distributions are shown for the indicated ranks.

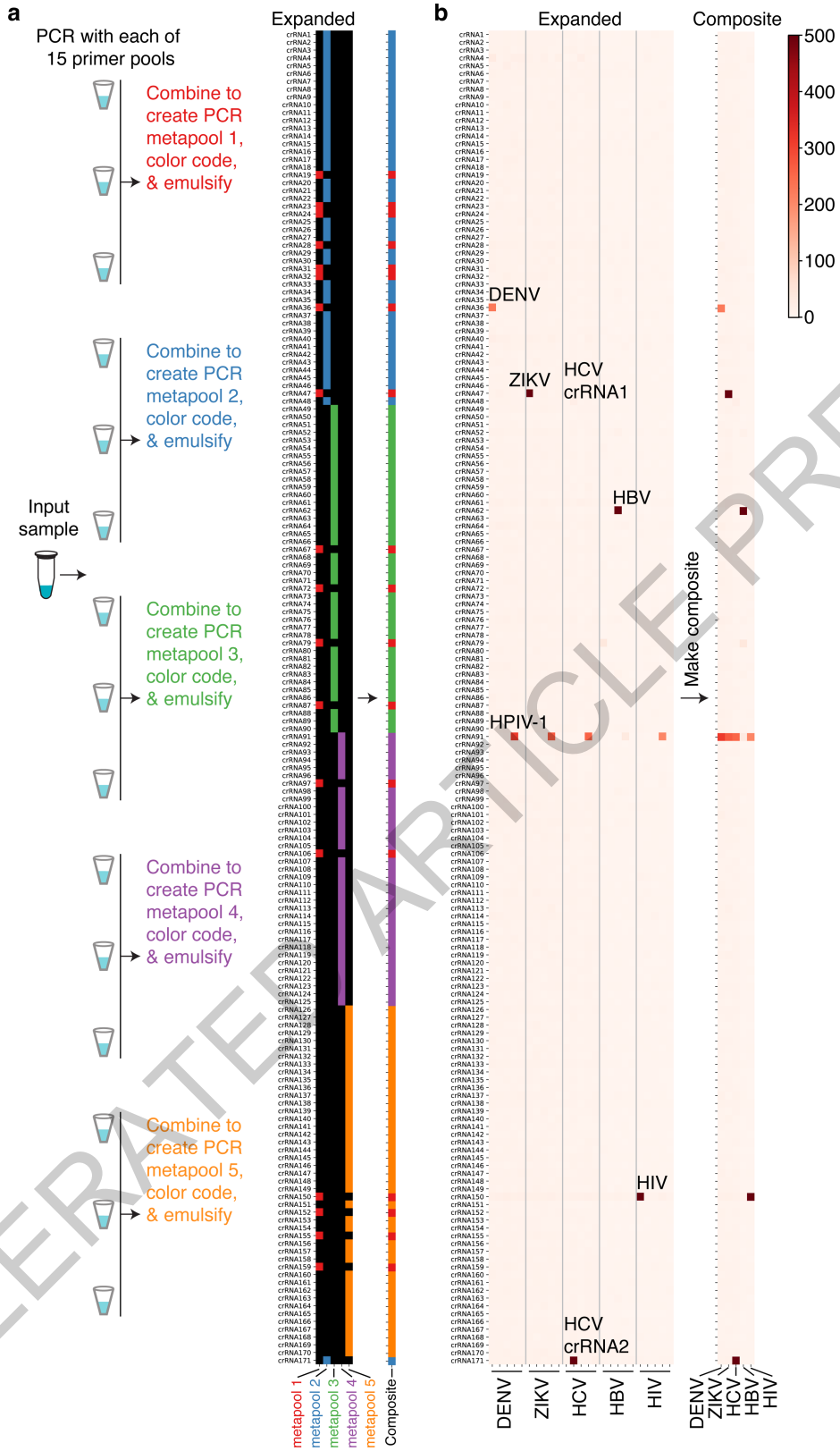

Extended Data Fig. 7 | Synthetic target testing with HV panel. a, Sample handling and data analysis for unknown samples. Following multiplexed PCR with 15 pools, PCR products are combined into sets of 3 (PCR metapools). A subset of the crRNAs correspond to the primers in each PCR metapool, shown by the colors in the expanded heatmap. Composite heatmaps are generated by combining data from the metapools in the expanded heatmap. **b**, Five synthetic targets (10^4 cp/µl) were amplified with all primer pools and detected using 169 crRNAs from the HV panel plus HCV crRNA 2. Heatmap indicates background-subtracted fluorescence after 1 hour. DENV: dengue virus; ZIKV: Zika virus; Flu A: influenza A virus; HIV: human immunodeficiency virus; HCV: hepatitis C virus.

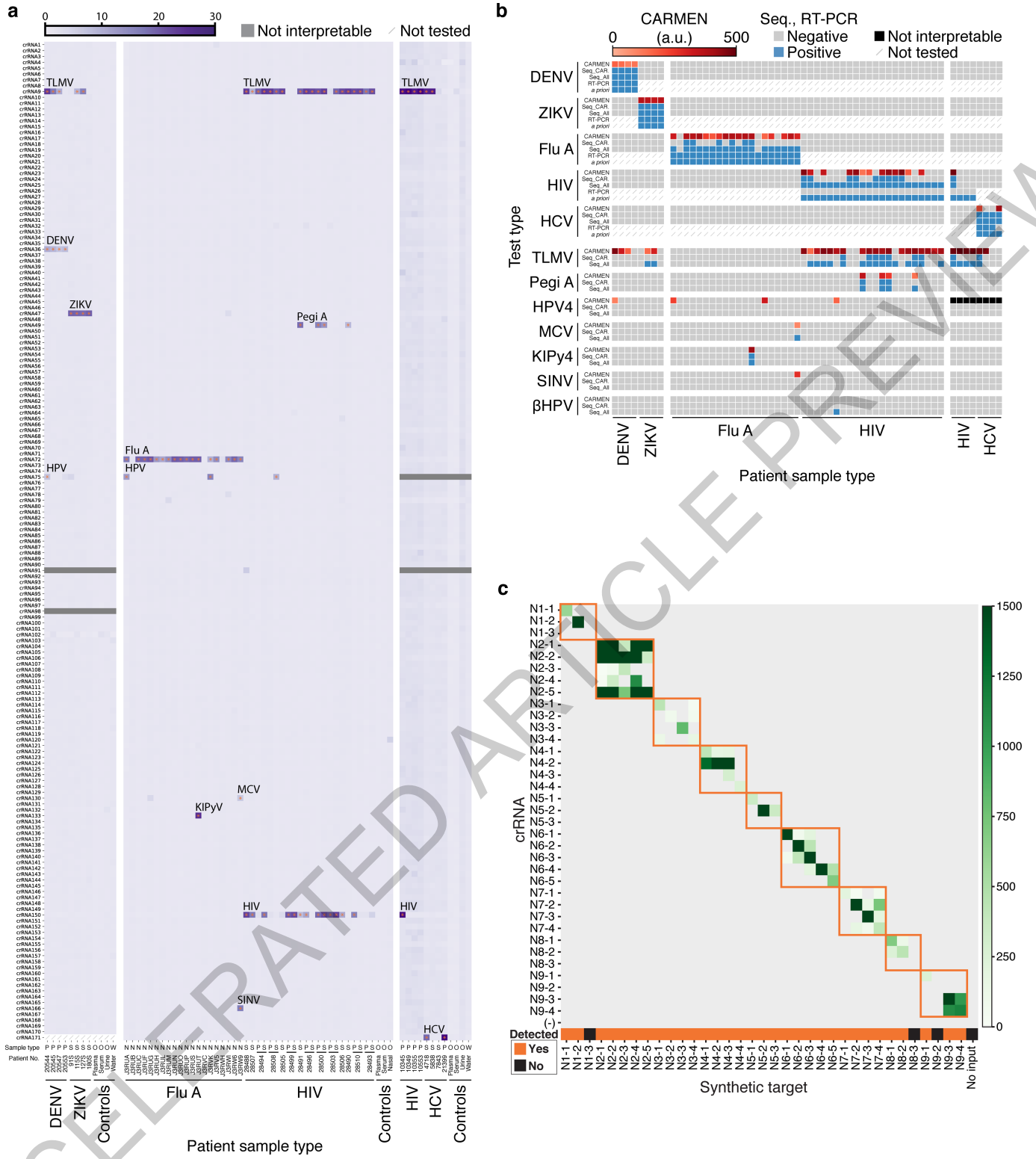

Extended Data Fig. 8 | See next page for caption.

Extended Data Fig. 8 | Clinical sample testing with HV panel and performance of Influenza A subtyping. a, CARMEN testing of patient samples and healthy pooled controls using the HV panel. Color bar indicates fold change above background at 1 hour for most crRNAs (3 hour time point is shown for HIV and HCV crRNAs). Tests that could not be interpreted due to the presence of signal above background in the negative controls are colored in dark gray (not interpretable). Sample types: N: throat/nasal swabs; O: pooled healthy controls; P: plasma; S: serum; W: water. Orange asterisks indicate signal above threshold 6-fold higher than background). **b**, Comparison of results from CARMEN, RNA sequencing-based identification of the sequence targeted by the indicated crRNA (Seq_CAR.), RNA sequencing-based identification of any sequences from the indicated virus (Seq_All), RT-PCR for the indicated virus, and *a priori* expectation based on information from the patient sample provider (*a priori*) for 4 dengue, 4 Zika, 20 influenza A, 26 HIV, and 4 HCV patient samples. CARMEN testing was done over three rounds (as indicated by vertical separation between sections). Threshold cutoffs for making calls were: CARMEN: 6-fold higher than background; Seq_CAR.: 2 reads; Seq_All: 1 read per million (RPM); RT-PCR: according to the manufacturer's instructions. Tests were considered uninterpretable when signal above background was observed in healthy pooled control samples assayed in parallel with patient samples. Heatmaps indicate background-subtracted fluorescence after 1 hour for most crRNAs (3 hour time point is shown for HIV and HCV crRNAs). DENV: dengue virus; ZIKV: Zika virus; Flu A: influenza A virus; HIV: human immunodeficiency virus; HCV: hepatitis C virus; TLMV: Torque teno-like mini virus; Pegi A: pegivirus A; HPV4: human papillomavirus 4; KIPyV: KI polyomavirus; MCV: Merkel cell polyomavirus; SINV: Sindbis virus, βHPV: beta human papillomavirus 2. **c**, Heatmap showing the full set of crRNAs designed to capture influenza N sequence diversity. We tested 35 synthetic targets (10^4 cp/µl) using 35 crRNAs. Gray: below detection threshold; Green: fluorescence counts above threshold; Orange outlines: subtypes; Lowest row displays which targets are detected. Time: 3 hours.

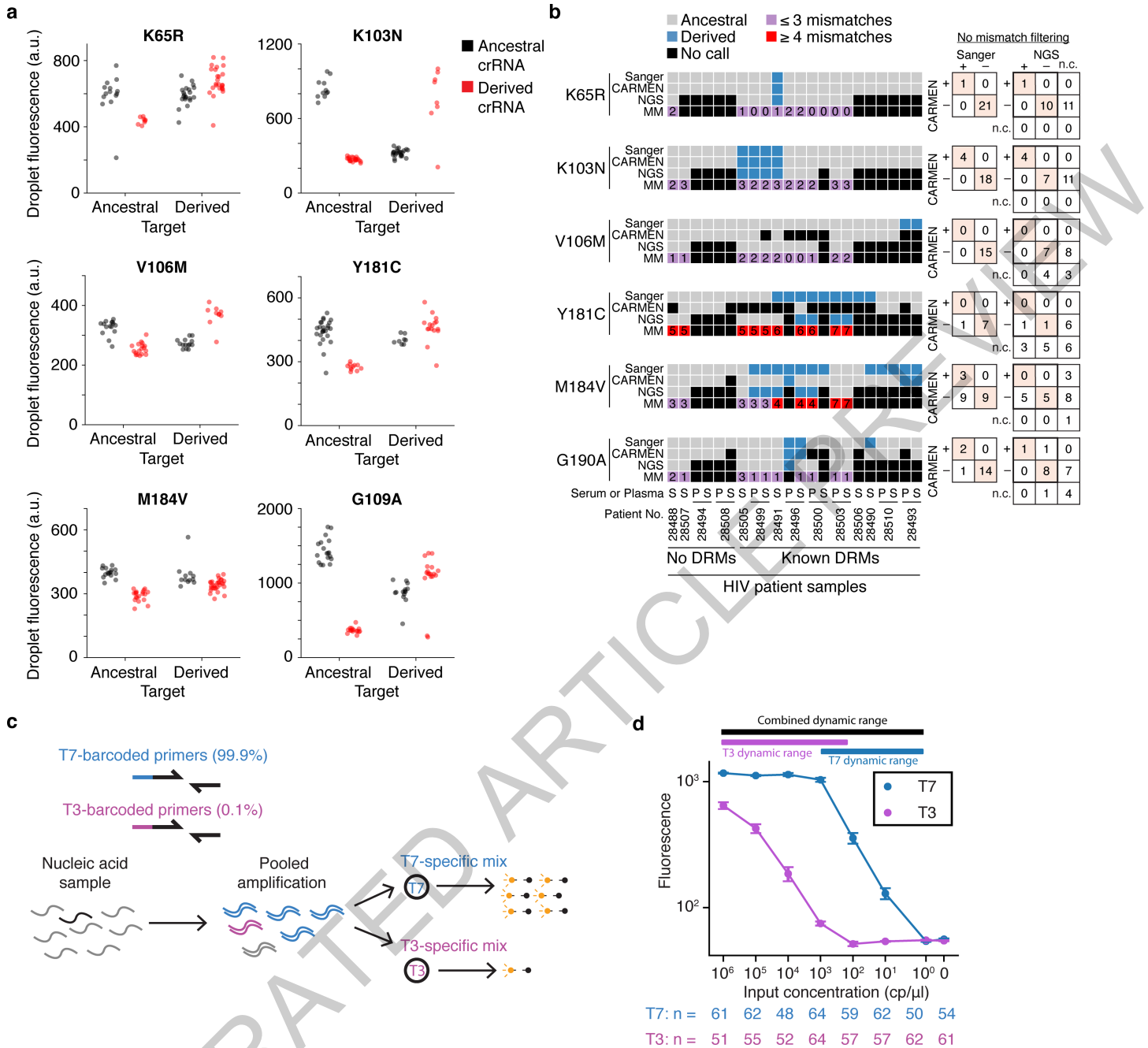

Extended Data Fig. 9 | HIV reverse transcriptase (RT) mutation detection and future directions for CARMEN-Cas13. a, Distributions of droplet fluorescence for each HIV RT crRNA-target pair after 30 min in most cases; 3 hour time point for V106M and M184V. SNP indices in Fig. 4b are calculated from the medians of these distributions. **b**, Comparison of prior expectation based on Sanger sequencing from the patient sample provider (Sanger), CARMEN testing (CARMEN), and next generation sequencing of RNA from each sample (NGS) for 22 patient samples infected with wildtype HIV (No DRMs) or HIV bearing known drug resistance mutations (Known DRMs). In some cases, NGS revealed a high number of mismatches (MM) between the HIV sequence in the sample and the crRNA sequence used in the CARMEN HIV RT DRM panel. Summary tables at the right quantify concordance between CARMEN and Sanger sequencing or CARMEN and NGS. **c**, Quantitative CARMEN-Cas13 schematic showing amplification primers containing T7 or T3 promoters, leading to increased signal for the majority (T7) product after Cas13 detection. **d**, Increased dynamic range of detection using quantitative CARMEN-Cas13. Dynamic range is indicated using colored bars above the graph. Error bars indicate SEM. Replicates (n) for T7 and T3 data are noted in color-coded text beneath the plot.

Extended Data Table 1 | Consumables cost calculation concerning CARMEN-Cas13

	Category	Cost (USD)	Notes	
	Fixed cost per chip	$16.00	Includes oil, surfactant, and chip itself	
	Marginal cost per sample	$2.24	Includes PCR reagents, droplet generation, and color codes	
	Marginal cost per detection mix	$5.34	Includes detection reagents, droplet generation, and color codes	
# samples	**# detection mixes**	**Number of tests**	**Total CARMEN cost (USD)**	**Cost per test (USD)**
20	20	400	$167.57	$0.42
100	50	5,000	$506.90	$0.10
200	100	20,000	$1,045.80	$0.05
SHERLOCK in a plate				
Cost per ul (USD)	**Detection volume (ul)**	**Replicates**	**Volume per test (ul)**	**Cost per test (USD)**
$0.06	20	4	92	$5.52

nature research

Corresponding author(s): Cameron Myhrvold and Paul Blainey

Last updated by author(s): February 26, 2020

Reporting Summary

Nature Research wishes to improve the reproducibility of the work that we publish. This form provides structure for consistency and transparency in reporting. For further information on Nature Research policies, see Authors & Referees and the Editorial Policy Checklist.

Statistics

For all statistical analyses, confirm that the following items are present in the figure legend, table legend, main text, or Methods section.

n/a	Confirmed
☐	☒ The exact sample size (*n*) for each experimental group/condition, given as a discrete number and unit of measurement
☐	☒ A statement on whether measurements were taken from distinct samples or whether the same sample was measured repeatedly
☐	☒ The statistical test(s) used AND whether they are one- or two-sided *Only common tests should be described solely by name; describe more complex techniques in the Methods section.*
☒	☐ A description of all covariates tested
☒	☐ A description of any assumptions or corrections, such as tests of normality and adjustment for multiple comparisons
☐	☒ A full description of the statistical parameters including central tendency (e.g. means) or other basic estimates (e.g. regression coefficient) AND variation (e.g. standard deviation) or associated estimates of uncertainty (e.g. confidence intervals)
☒	☐ For null hypothesis testing, the test statistic (e.g. *F*, *t*, *r*) with confidence intervals, effect sizes, degrees of freedom and *P* value noted *Give P values as exact values whenever suitable.*
☒	☐ For Bayesian analysis, information on the choice of priors and Markov chain Monte Carlo settings
☒	☐ For hierarchical and complex designs, identification of the appropriate level for tests and full reporting of outcomes
☒	☐ Estimates of effect sizes (e.g. Cohen's *d*, Pearson's *r*), indicating how they were calculated

Our web collection on statistics for biologists contains articles on many of the points above.

Software and code

Policy information about availability of computer code

Data collection	Matlab 2013 for microscope and camera control
Data analysis	Python 2.7, custom analysis code available at github akulesa/kchip, mafft v7.31 was used for primer and crRNA sequence design

For manuscripts utilizing custom algorithms or software that are central to the research but not yet described in published literature, software must be made available to editors/reviewers. We strongly encourage code deposition in a community repository (e.g. GitHub). See the Nature Research guidelines for submitting code & software for further information.

Data

Policy information about availability of data

All manuscripts must include a data availability statement. This statement should provide the following information, where applicable:

- Accession codes, unique identifiers, or web links for publicly available datasets
- A list of figures that have associated raw data
- A description of any restrictions on data availability

Viral genome alignments and sequencing data will be made publicly available. Raw data may be made available upon request.

Field-specific reporting

Please select the one below that is the best fit for your research. If you are not sure, read the appropriate sections before making your selection.

☒ Life sciences ☐ Behavioural & social sciences ☐ Ecological, evolutionary & environmental sciences

For a reference copy of the document with all sections, see nature.com/documents/nr-reporting-summary-flat.pdf

Life sciences study design

All studies must disclose on these points even when the disclosure is negative.

Sample size	The number of replicates necessary to make a call was determined by bootstrap, as described in the Supplementary Discussion. Sample sizes were the result of stochastic loading of microwell arrays, as described in the Supplementary Discussion.
Data exclusions	Droplets data were quality filtered for size of droplet (excluding any droplets that may merge across wells or fail to merge) and for the distance between the droplet's color coordinates and those of its assigned color code cluster (excluding droplets where the color code cluster assignment is very uncertain). Exclusions were made based on pre-established quality control filters. Low-quality data were droplets that fell outside of a minimum radius from a cluster, making their cluster assignment ambiguous. By applying a distance filter (illustrated in EDF 5), we remove low-quality data. The cutoff for the distance filter is pre-established based on testing the droplet color codes without samples.
Replication	Each experiment includes at least 3 technical replicates per data point, with a median of 10-15 replicates. Biological replicates were consistent (97% concordance between the replicates of the HAV tests, Ex. Data Fig. 6). Replicates for main text figures are provided in Supplementary File 6.
Randomization	Samples were not randomized into groups, as samples were not grouped.
Blinding	Blinding was performed for the HIV clinical samples for DRM testing, but not for other samples. Blinding was not possible for some samples due to the nature of the patient cohorts selected (they were known to be disease-positive)

Reporting for specific materials, systems and methods

We require information from authors about some types of materials, experimental systems and methods used in many studies. Here, indicate whether each material, system or method listed is relevant to your study. If you are not sure if a list item applies to your research, read the appropriate section before selecting a response.

Materials & experimental systems

n/a	Involved in the study
☒	☐ Antibodies
☒	☐ Eukaryotic cell lines
☒	☐ Palaeontology
☒	☐ Animals and other organisms
☒	☐ Human research participants
☒	☐ Clinical data

Methods

n/a	Involved in the study
☒	☐ ChIP-seq
☒	☐ Flow cytometry
☒	☐ MRI-based neuroimaging